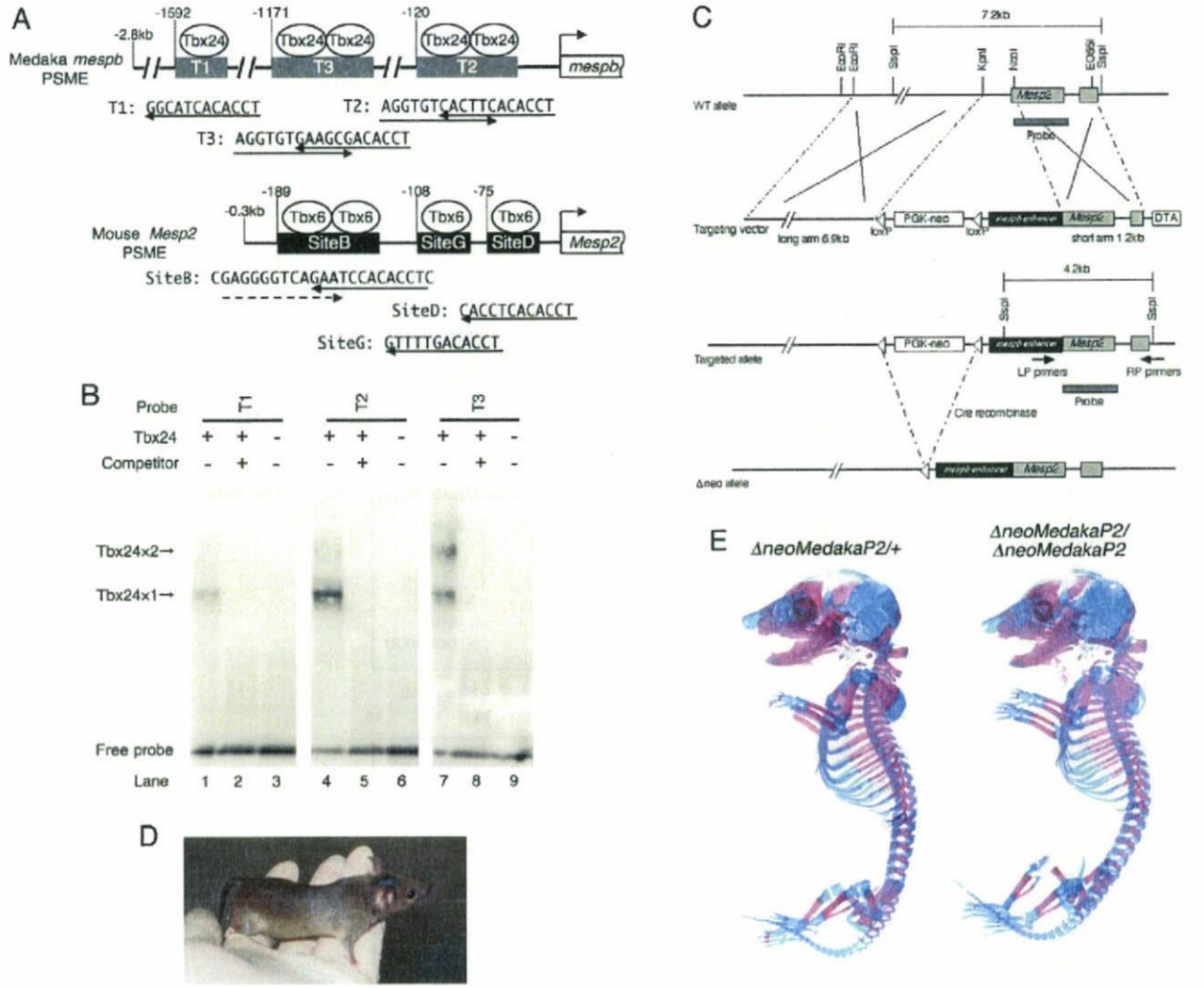

Fig. 4. The medaka *mespb* PSM enhancer is functionally equivalent to its counterpart in the mouse. (**A**) A comparison of the medaka *mespb* and mouse *Mesp2* PSME regions. Black and gray boxes represent presumptive T-box binding sites. The numbers above the boxes represent the nucleotide positions from the first ATG. The nucleotide sequences of the putative T-box binding sequences are shown beneath. Consensus Tbx6 binding sequences and their directions are indicated by arrows. The dashed arrow in Site B of the *Mesp2* PSME depicts an incomplete Tbx6 binding sequence that only binds to Tbx6 if an adjoining complete Tbx6 binding sequence is present. The T-box proteins that might bind to these sequences are indicated. (**B**) EMSA analysis of the T-box binding sites in the medaka *mespb* PSME. T-box binding site T1 associates with a single Tbx24 molecule and T2 and T3 with two Tbx24 molecules, which is consistent with their nucleotide sequences as shown in A. (**C**) The targeting strategy used to generate the medaka *mespb* PSME knock-in mouse (*medakaP2*). A 2.8-kb fragment of *mespb* genomic DNA that is required for PSM-specific *mespb* expression was substituted for *Mesp2* PSME by homologous recombination. The neoR selection marker was removed by recombination using the Cre-loxP system. (**D**) *medakaP2* homozygotes are viable and have normal external features. (**E**) Homozygotes are indistinguishable from heterozygotes and wild-type littermates in skeletal preparations.

by which Tbx6 regulates its target genes together with various partners remain elusive, it is possible that the number and spatial organization of Tbx6 binding sites facilitate the response of P2PSME to Notch signaling.

In total, there are four Tbx6 binding sequences in this region: two palindrome-like sequences in Site B and one each in Sites D and G. Importantly, the P2PSME reporters with only one intact Tbx6 binding site were inactive in both the luciferase assay and the transgenic analyses (Fig. 3D), suggesting that a single P2PSME-bound Tbx6 molecule might not act as a mediator of Notch signaling in the regulatory mechanism controlling *Mesp2* expression. This is consistent with the observation that Site G fails to activate *Mesp2* expression by itself in the *P2EmB1D* mouse.

The loss of two or more of the four Tbx6 binding sites greatly diminishes P2PSME activity in both luciferase and transgenic assays (Fig. 3D). Interestingly, the reporters with two intact Tbx6 binding sites showed varied levels of activity depending upon the position of the intact sites. Two intact Tbx6 binding sites in Site B resulted in the highest reporter activity (Fig. 3D). These data indicate that Site B may be of predominant importance in the function of P2PSME,

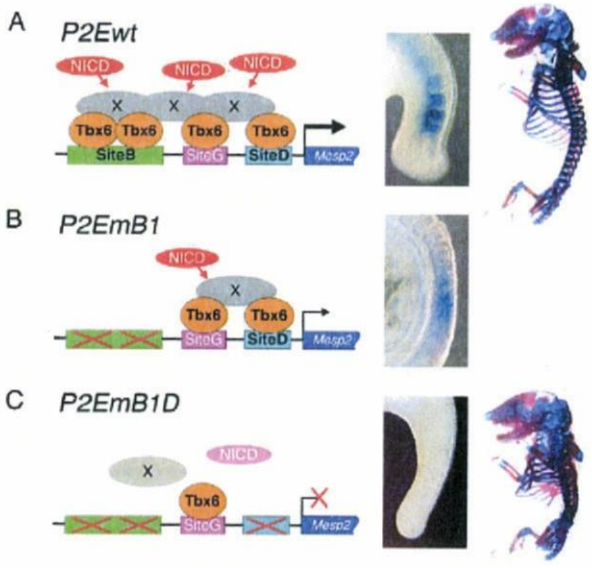

Fig. 5. Putative mechanism for the Tbx6-mediated regulation of Mesp genes. (**A**) Tbx6 activates *Mesp2* expression through multiple Tbx6 binding sites. Notch signaling (NICD, red ovals) activates *Mesp2* expression via factor X (gray ovals), which recognizes two neighboring Tbx6 binding sites in P2PSME. (Left) Schematic description of the Tbx6-dependent activation of *Mesp2*. (Middle column) *lacZ* expression in the P2Ewt transgenic embryo. (Right) Normal skeletal formation in the heterozygous fetus of a *P2EmB1D* mouse. (**B**) Mutation in Site B results in decreased expression of *Mesp2*. (**C**) A single Tbx6 binding site is unable to activate *Mesp2* expression, presumably owing to an inability to respond to Notch signaling.

implying that its two neighboring Tbx6 binding sites play a central role in regulating the activation of *Mesp2*. The binding of Tbx6 to one of the two binding sites in Site B depends on the presence of another Tbx6 molecule binding to this site (Yasuhiko et al., 2006). This property might be related to the unique palindrome-like sequence of this site. Although several T-box binding sites have been identified in the upstream region of other Tbx6-downstream genes, such as *Dll1* (Hofmann et al., 2004) and *Msgn1* (Wittler et al., 2007), the palindrome-like site has thus far been found only in the PSME of *Mesp2* and its medaka ortholog *mespb* (Fig. 4A). It is therefore possible that two neighboring Tbx6 molecules on the palindrome-like site are specifically recognized by as yet unidentified factor(s) (Fig. 5, 'X') that together with Tbx6 constitutes an RBPJ-κ (Rbpj)-independent Notch signaling machinery [disruption of potential RBPJ-κ binding sites does not affect P2PSME activity in transgenic embryos (Yasuhiko et al., 2006)]. Further analyses of *Mesp2* PSME might shed light on these novel regulatory mechanisms that operate during development.

Mutations that removed any one of the Tbx6 binding sites in P2PSME, regardless of which, diminished luciferase reporter activity by the same amount (Fig. 3C), suggesting that each Tbx6 binding site contributes equally to *Mesp2* expression in vitro. In vivo, by contrast, the mutation of a single Tbx6 binding site did not seem to affect PSM-specific gene expression (Fig. 3C). Taken together, these results indicate that the multiple Tbx6 binding sites confer a functional robustness to P2PSME that ensures proper *Mesp2* expression during embryogenesis.

An evolutionally conserved mechanism regulating Mesp expression through multiple T-box binding sites

We previously found that the deletion of two T-box binding sites in the *mespb* PSME greatly reduced its PSM-specific enhancer activity in transgenic medaka embryos (Terasaki et al., 2006), similar to our findings in transgenic mouse embryos. The medaka *mespb* PSME harbors three T-box binding sites (T1-T3), which is similar to the complement of the mouse *Mesp2* PSME (Fig. 4A). However, the total length of the PSME is very different between mouse *Mesp2* and medaka *mespb* (356 bp versus 2.8 kb, respectively) (Terasaki et al., 2006). The number of T-box proteins that bind to the medaka and mouse PSMEs is also different (Fig. 4A,B), and the distance between each element is greater in the *mespb* PSME than in its mouse counterpart.

We have demonstrated, however, that the medaka *mespb* PSME is functionally equivalent to the mouse *Mesp2* PSME. In our transgenic assay, a mutation in the double T-box binding site (Site B in mouse and Site T2 in medaka) had the most profound effect upon PSME activity. Consistent with these results, deletion of medaka Site T1 (harboring a single T-box binding sequence) did not affect reporter gene expression. However, deletion of one of the sites within the double T-box binding sequence (T2) caused a 50% decrease in reporter expression (Terasaki et al., 2006), again demonstrating the importance of the binding to the double T-box site for PSM enhancer function.

In the teleost fish, zebrafish, the T-box transcription factor Tbx24 was identified as responsible for the fused somite (*fss*) mutant phenotype. Tbx24 has a T-box domain that is homologous to that of mouse Tbx6 (Nikaido et al., 2002). The segmentation of somites and expression of *mespb* are eliminated in the *fss* mutant (Sawada et al., 2000), implying that *mespb* is a downstream target of Tbx24, similar to the relationship between *Mesp2* and Tbx6 in mice. However, *fss* mutant fish are viable and fertile (van Eeden et al., 1996), whereas *Tbx6*-null mouse embryos fail to form a mesoderm and die early in development (Chapman and Papaioannou, 1998). This difference might be due to the presence in zebrafish of a *Tbx6* counterpart gene, *spadetail*, which supports paraxial mesoderm formation. Despite this difference, our data clearly demonstrate that the mechanism regulating the PSM-specific expression of *Mesp2* and *mespb* is evolutionarily well conserved between fish and mice.

We thank Hiroyuki Takeda (University of Tokyo) for providing Tbx24 cDNA clones and Mariko Ikumi, Eriko Ikeno and Shunsuke Matsusaka for technical assistance. This work was supported by a grant-in-aid for scientific research from the Ministry of Education, Culture, Sports, Science and Technology, Japan, a grant for Research on Risk on Chemical Substances (H20-004) from the Ministry of Health, Labor and Welfare of Japan, and a grant from the NIG Cooperative Research Program (2007-B66).

References

Bussen, M., Petry, M., Schuster-Gossler, K., Leitges, M., Gossler, A. and Kispert, A. (2004). The T-box transcription factor Tbx18 maintains the separation of anterior and posterior somite compartments. *Genes Dev.* **18**, 1209-1221.

Chapman, D. L. and Papaioannou, V. E. (1998). Three neural tubes in mouse embryos with mutations in the T-box gene Tbx6. *Nature* **391**, 695-697.

Chapman, D. L., Agulnik, I., Hancock, S., Silver, L. M. and Papaioannou, V. E. (1996). Tbx6, a mouse T-Box gene implicated in paraxial mesoderm formation at gastrulation. *Dev. Biol.* **180**, 534-542.

Delfini, M. C., Dubrulle, J., Malapert, P., Chal, J. and Pourquie, O. (2005). Control of the segmentation process by graded MAPK/ERK activation in the chick embryo. *Proc. Natl. Acad. Sci. USA* **102**, 11343-11348.

Dunty, W. C., Jr, Biris, K. K., Chalamalasetty, R. B., Taketo, M. M., Lewandoski, M. and Yamaguchi, T. P. (2008). Wnt3a/β-catenin signaling controls posterior body development by coordinating mesoderm formation and segmentation. *Development* **135**, 85-94.

Galceran, J., Sustmann, C., Hsu, S. C., Folberth, S. and Grosschedl, R. (2004). LEF1-mediated regulation of Delta-like1 links Wnt and Notch signaling in somitogenesis. *Genes Dev.* **18**, 2718-2723.
Haraguchi, S., Kitajima, S., Takagi, A., Takeda, H., Inoue, T. and Saga, Y. (2001). Transcriptional regulation of Mesp1 and Mesp2 genes: differential usage of enhancers during development. *Mech. Dev.* **108**, 59-69.
Hitachi, K., Kondow, A., Danno, H., Inui, M., Uchiyama, H. and Asashima, M. (2008). Tbx6, Thylacine1, and E47 synergistically activate bowline expression in Xenopus somitogenesis. *Dev. Biol.* **313**, 816-828.
Hofmann, M., Schuster-Gossler, K., Watabe-Rudolph, M., Aulehla, A., Herrmann, B. G. and Gossler, A. (2004). WNT signaling, in synergy with T/TBX6, controls Notch signaling by regulating Dll1 expression in the presomitic mesoderm of mouse embryos. *Genes Dev.* **18**, 2712-2717.
Hogan, B., Beddington, R., Costantini, F. and Lacy, E. (1994). *Manipulating the Mouse Embryo: a Laboratory Manual*. Cold Spring Harbor, NY: Cold Spring Harbor Laboratory Press.
Moreno, T. A. and Kintner, C. (2004). Regulation of segmental patterning by retinoic acid signaling during Xenopus somitogenesis. *Dev. Cell* **6**, 205-218.
Morimoto, M., Takahashi, Y., Endo, M. and Saga, Y. (2005). The Mesp2 transcription factor establishes segmental borders by suppressing Notch activity. *Nature* **435**, 354-359.
Morimoto, M., Kiso, M., Sasaki, N. and Saga, Y. (2006). Cooperative Mesp activity is required for normal somitogenesis along the anterior-posterior axis. *Dev. Biol.* **300**, 687-698.
Nikaido, M., Kawakami, A., Sawada, A., Furutani-Seiki, M., Takeda, H. and Araki, K. (2002). Tbx24, encoding a T-box protein, is mutated in the zebrafish somite-segmentation mutant fused somites. *Nat. Genet.* **31**, 195-199.
Nomura-Kitabayashi, A., Takahashi, Y., Kitajima, S., Inoue, T., Takeda, H. and Saga, Y. (2002). Hypomorphic Mesp allele distinguishes establishment of rostrocaudal polarity and segment border formation in somitogenesis. *Development* **129**, 2473-2481.
Oginuma, M., Niwa, Y., Chapman, D. L. and Saga, Y. (2008). Mesp2 and Tbx6 cooperatively create periodic patterns coupled with the clock machinery during mouse somitogenesis. *Development* **35**, 2555-2562.
Rupp, R. A., Snider, L. and Weintraub, H. (1994). Xenopus embryos regulate the nuclear localization of XMyoD. *Genes Dev.* **8**, 1311-1323.
Saga, Y. and Takeda, H. (2001). The making of the somite: molecular events in vertebrate segmentation. *Nat. Rev. Genet.* **2**, 835-845.
Saga, Y., Yagi, T., Ikawa, Y., Sakakura, T. and Aizawa, S. (1992). Mice develop normally without tenascin. *Genes Dev.* **6**, 1821-1831.
Saga, Y., Hata, N., Koseki, H. and Taketo, M. M. (1997). Mesp2: a novel mouse gene expressed in the presegmented mesoderm and essential for segmentation initiation. *Genes Dev.* **11**, 1827-1839.
Sasaki, H. and Hogan, B. L. (1996). Enhancer analysis of the mouse HNF-3 beta gene: regulatory elements for node/notochord and floor plate are independent and consist of multiple sub-elements. *Genes Cells* **1**, 59-72.
Sawada, A., Fritz, A., Jiang, Y. J., Yamamoto, A., Yamasu, K., Kuroiwa, A., Saga, Y. and Takeda, H. (2000). Zebrafish Mesp family genes, mesp-a and mesp-b are segmentally expressed in the presomitic mesoderm, and Mesp-b confers the anterior identity to the developing somites. *Development* **127**, 1691-1702.
Takahashi, Y., Koizumi, K., Takagi, A., Kitajima, S., Inoue, T., Koseki, H. and Saga, Y. (2000). Mesp2 initiates somite segmentation through the Notch signalling pathway. *Nat. Genet.* **25**, 390-396.
Takahashi, Y., Inoue, T., Gossler, A. and Saga, Y. (2003). Feedback loops comprising Dll1, Dll3 and Mesp2, and differential involvement of Psen1 are essential for rostrocaudal patterning of somites. *Development* **130**, 4259-4268.
Takahashi, Y., Yasuhiko, Y., Kitajima, S., Kanno, J. and Saga, Y. (2007). Appropriate suppression of Notch signaling by Mesp factors is essential for stripe pattern formation leading to segment boundary formation. *Dev. Biol.* **304**, 593-603.
Terasaki, H., Murakami, R., Yasuhiko, Y., Shin, I. T., Kohara, Y., Saga, Y. and Takeda, H. (2006). Transgenic analysis of the medaka mesp-b enhancer in somitogenesis. *Dev. Growth Differ.* **48**, 153-168.
van Eeden, F. J., Granato, M., Schach, U., Brand, M., Furutani-Seiki, M., Haffter, P., Hammerschmidt, M., Heisenberg, C. P., Jiang, Y. J., Kane, D. A. et al. (1996). Mutations affecting somite formation and patterning in the zebrafish, Danio rerio. *Development* **123**, 153-164.
White, P. H. and Chapman, D. L. (2005). Dll1 is a downstream target of Tbx6 in the paraxial mesoderm. *Genesis* **42**, 193-202.
Wittler, L., Shin, E. H., Grote, P., Kispert, A., Beckers, A., Gossler, A., Werber, M. and Herrmann, B. G. (2007). Expression of Msgn1 in the presomitic mesoderm is controlled by synergism of WNT signalling and Tbx6. *EMBO Rep.* **8**, 784-789.
Yagi, T., Tokunaga, T., Furuta, Y., Nada, S., Yoshida, M., Tsukada, T., Saga, Y., Takeda, N., Ikawa, Y. and Aizawa, S. (1993). A novel ES cell line, TT2, with high germline-differentiating potency. *Anal. Biochem.* **214**, 70-76.
Yasuhiko, Y., Haraguchi, S., Kitajima, S., Takahashi, Y., Kanno, J. and Saga, Y. (2006). Tbx6-mediated Notch signaling controls somite-specific Mesp2 expression. *Proc. Natl. Acad. Sci. USA* **103**, 3651-3656.

FEBS Letters 582 (2008) 3935–3940

Involvement of Sema4A in the progression of experimental autoimmune myocarditis

Nobuhiko Makino[a,b,c], Toshihiko Toyofuku[b,c,*], Noriko Takegahara[b,c], Hyota Takamatsu[b,c], Tatsusada Okuno[b,c], Yukinobu Nakagawa[b,c,e], Sujin Kang[b,c], Satoshi Nojima[b,c,f], Masatsugu Hori[a,h], Hitoshi Kikutani[c,d,g], Atsushi Kumanogoh[b,c,*]

[a] *Department of Cardiovascular Medicine, Osaka University Graduate School of Medicine, 2-2 Yamada-oka, Suita, Osaka 565-0871, Japan*
[b] *Department of Immunopathology, Research Institute for Microbial Diseases, Osaka University, 3-1 Yamada-oka, Suita, Osaka 565-0871, Japan*
[c] *World Premier International Immunology Frontier Research Center, Osaka University, 3-1 Ymada-oka, Suita, Osaka 565-0871, Japan*
[d] *Department of Molecular Immunology, Research Institute for Microbial Diseases, Osaka University, 3-1 Yamada-oka, Suita, Osaka 565-0871, Japan*
[e] *Department of Dermatology, Osaka University Graduate School of Medicine, 2-2 Yamadoka, Suita, Osaka 565-087, Japan*
[f] *Department of Pathology, Osaka University Graduate School of Medicine, 2-2 Yamada-oka, Suita, Osaka 565-0871, Japan*
[g] *CREST, Japan Science and Technology Corporation, Japan*
[h] *Osaka Medical Center for Cancer and Cardiovascular Diseases, 1-3-3 Nakamichi, Higashinari-ku, Osaka 537-8511, Japan*

Received 2 October 2008; revised 23 October 2008; accepted 24 October 2008

Available online 31 October 2008

Edited by Masayuki Miyasaka

Abstract Dilated cardiomyopathy often results from autoimmunity triggered by microbial infections during myocarditis. However, it remains unclear how immunological disorders are implicated in pathogenesis of autoimmune myocarditis. Here, we demonstrated that Sema4A, a class IV semaphorin, plays key roles in experimental autoimmune myocarditis (EAM). Dendritic cells pulsed with myosin heavy chain-α peptides induced severe myocarditis in wild-type mice, but not in Sema4A-deficient mice. In adoptive transfer experiments, $CD4^+$ T-cells from wild-type mice induced severe myocarditis, while $CD4^+$ T-cells from Sema4A-deficient mice exhibited considerably attenuated myocarditis. Our results indicated that Sema4A is critically involved in EAM by regulating differentiation of T-cells.

Keywords: Autoimmune myocarditis; Semaphorin; Dilated cardiomyopathy; Autoimmunity

1. Introduction

Myocarditis is an inflammatory heart disease that can be initiated by infectious pathogens, which is a frequent cause of cardiac disease among young adults. Myocarditis often results from infections with enteroviruses such as coxsackievirus B3 or adenoviruses [1]. In addition, cardiotropic bacteria such as Borrelia and Chlamydia can induce myocarditis and heart failure. Cumulative evidence suggests that myocarditis is a precursor of dilated cardiomyopathy (DCM), the major cause of heart failure and heart transplantation [1]. It has been suggested that autoimmune responses to cardiac antigens that are exposed after heart damage play a crucial role in prolonged damage of the myocardium, which promotes the development of DCM [2]. In fact, many affected individuals develop heart antigen-specific autoantibody responses and immunosuppressive therapy can improve heart function in DCM patients who have no evidence of viral or bacterial genomes in heart biopsies. In addition, peripheral blood lymphocytes from DCM patients can adoptively transfer the disease to severe combined immunodeficiency (SCID) mice lacking T- and B-cells [3]. Collectively, these findings strongly suggest that post-infectious autoimmunity is involved in DCM development. However, it has not been fully elucidated how pathogenic autoimmunity is triggered in myocarditis, making it difficult to treat myocarditis by immunosuppression.

Experimental autoimmune myocarditis (EAM) is a model of post-infectious myocarditis. EAM can be induced in susceptible mouse strains by immunizing with self-peptides derived from the myosin α heavy chain (MyHC-α) together with a strong adjuvant [4], or by injecting MyHC-α-loaded dendritic cells (DCs) [5]. Collectively, these findings imply that immune tolerance is broken by damage during infection, resulting in the release of self-antigens, the activation of DCs, and the subsequent activation of autoreactive T-cells. Consistent with this hypothesis, it has been demonstrated that EAM is a T-cell mediated autoimmune disease that can be transferred by $CD4^+$ T-cells from EAM mice [5]. Traditionally, $CD4^+$ T-cells have been divided into two subsets, Interferon-γ (IFN-γ)-producing type 1 helper T-cells (T_H1) and interleukin (IL)-4-, IL-10-, and IL-13-producing T_H2 cells. It has been assumed that the T_H1/ T_H2 cytokine balance is important in the development of myocarditis [6]. Recently, this model has been challenged by the identification of the IL-17-producing T_H17 cell subset, which has been shown to be involved in various models of immune-mediated tissue injury [7]. In addition, it has been reported that immuno-regulatory cytokines such as IL-10

*Corresponding authors. Department of Immunopathology, Research Institute for Microbial Diseases, Osaka University, 3-1 Yamada-oka, Suita, Osaka 565-0871, Japan. Fax: +81 6 6879 8332.
E-mail addresses: toyofuku@ragtime.biken.osaka-u.ac.jp (T. Toyofuku), kumanogo@ragtime.biken.osaka-u.ac.jp (A. Kumanogoh).

Abbreviations: DCM, dilated cardiomyopathy; SCID, severe combined immunodeficiency; EAM, experimental autoimmune myocarditis; MyHC-α, myosin α heavy chain; DCs, dendritic cells; IFN-γ, Interferon-γ; T_H1, type 1 helper T-cells; IL, interleukin; Tim-2, T-cell, immunoglobulin and mucin domain protein 2; EAE, experimental autoimmune encephalomyelitis; Treg, regulatory T-cells; Foxp3, forkhead box P3

0014-5793/$34.00
doi:10.1016/j.febslet.2008.10.040

[8,9] and IL-13 [10] can ameliorate EAM development. In this context, the precise mechanism of $CD4^+$ T-cells in the development of EAM remains unclear.

Semaphorins were originally identified as axon guidance factors during neuronal development [11]. In recent years, semaphorins have emerged as important factors that have diverse and critical functions in other physiological processes, including heart morphogenesis, vascular growth, tumor progression, and immune cell regulation. In particular, cumulative evidence indicates that semaphorins are crucially involved in various phases of the immune response [12,13]. The class IV semaphorin subfamily member, Sema4A, regulates T-cell–mediated immune responses by interacting with its receptor Tim-2 (T-cell, immunoglobulin and mucin domain protein 2) which is expressed on T_H2 cells as a negative regulator [14–16]. Sema4A expression is specifically induced on the cell surface of T_H1 cells during helper T-cell differentiation. We previously reported that T-cell derived Sema4A is necessary for regulating T-cell differentiation. In fact, Sema4A-deficient mice have impaired T_H1-responses but rather enhanced T_H2-responses. Furthermore, anti-Sema4A antibody treatment attenuated the development of experimental autoimmune encephalomyelitis (EAE), which is a T-cell mediated disease. In this context, Sema4A is potentially a strong therapeutic target for T-cell mediated diseases.

In this study, we show that Sema4A-deficient mice are resistant to the development of EAM, and that a disregulated balance of helper T-cells is responsible for this resistance. Our findings suggest that Sema4A is a potential therapeutic target for autoimmune myocarditis.

2. Materials and methods

2.1. Mice

BALB/c and SCID mice were purchased from Nippon Clea (Japan). BALB/c Sema4A-deficient mice were generated as described previously [14]. Six- to ten-week-old mice were used for all experiments. Mice were maintained in a specific pathogen free environment. All experimental procedures complied with our institutional guidelines.

2.2. Induction of autoimmune myocarditis

Immature bone marrow-derived DCs were generated as described previously [17]. Immature DCs were pulsed overnight with 10 μg/ml of mouse MyHC-α (amino acids 614–629) (Ac-**R**SLKLMATLF-STYASAD**R**-OH; purity >95%; Biologica, Japan). Bold letters indi-

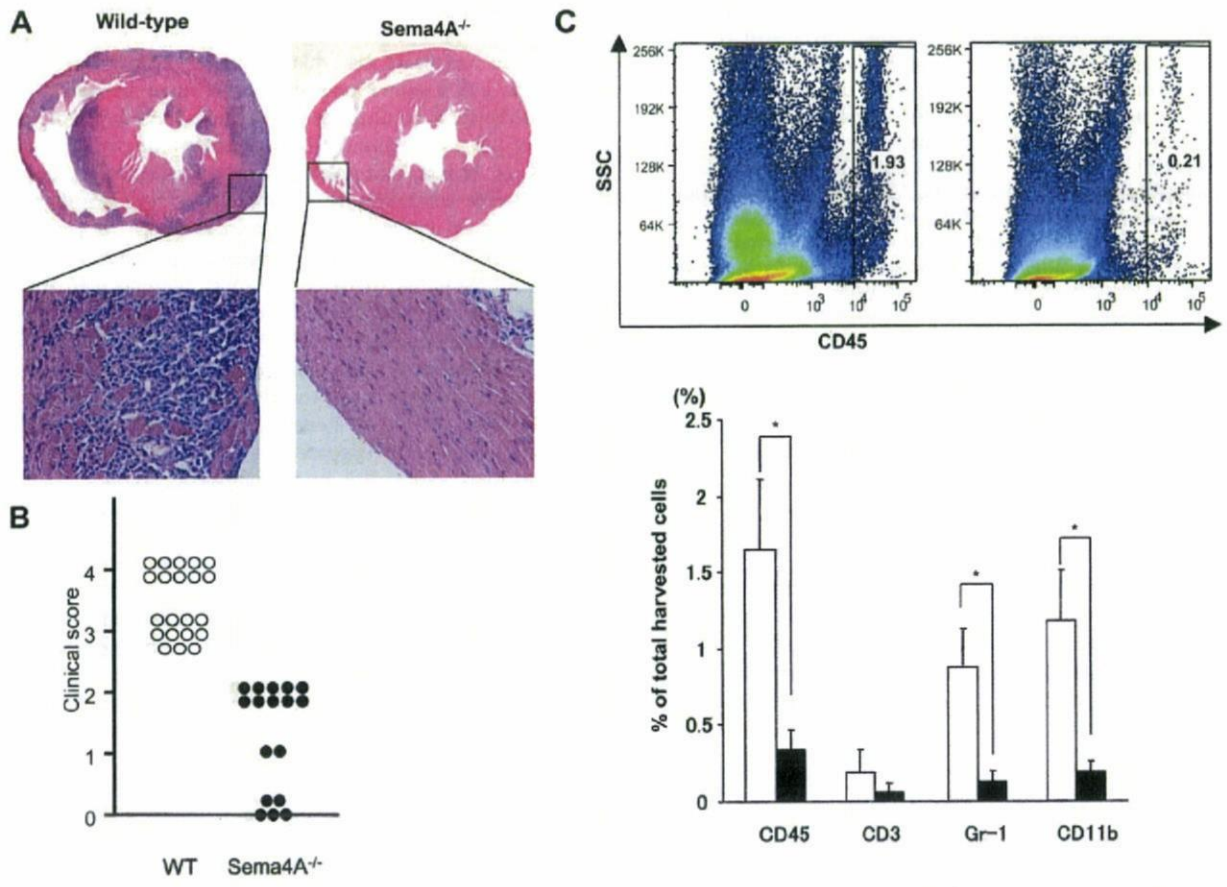

Fig. 1. Sema4A-deficient mice were resistant to EAM. (A) Autoimmune myocarditis was induced by immunizing with activated, MyHC-α loaded DCs. Severe myocarditis was observed in wild-type mice (left), while Sema4A-deficient mice were resistant to EAM (right). (B) Sema4A-deficient mice were resistant to EAM. Disease severity scores of individual wild-type (open circles) and Sema4A-deficient (closed circles) mice immunized with activated, MyHC-α loaded DCs. (C) The number of heart-infiltrating inflammatory cells was decreased in EAM-induced in Sema4A-deficient mice (upper). Heart-infiltrating cells were isolated from the hearts of wild-type (left) or Sema4A-deficient (right) mice 10 days after immunization with activated, MyHC-α loaded DCs. Cells were analyzed by flow cytometry, and a CD45/side scatter plot was used to determine the percentage of $CD45^+$ leukocytes (lower). The cellular composition of the heart infiltrate in immunized wild-type (white bars) or Sema4A-deficient (black bars) mice. The results are representative of five independent experiments.

cate the arginines that were included at both ends of the MyHC-α peptide to increase solubility [18]. DCs were treated with LPS (1 μg/ml, *Escherichia coli* 0111:B4; Sigma) and an anti-CD40 antibody (5 μg/ml, clone 3/23, BD PharMingen, USA) for 4 h. DCs were intraperitoneally injected into wild-type or Sema4A-deficient mice (1×10^5 cells/mouse) on days 0, 2 and 4.

2.3. Histopathology

On day 10, mice were killed and their hearts were removed, fixed in 10% neutral buffered formalin, and processed for hematoxylin and eosin staining. Myocarditis was scored on a scale from 0 to 4 (0, no infiltration of inflammatory cells; 1, small foci of inflammatory cells between myocytes; 2, larger foci of >100 inflammatory cells; 3, >10% of a cross section has inflammation; 4, >30% of a cross section has inflammation).

2.4. In vitro restimulation of $CD4^+$ T-cells

$CD4^+$ T-cells were purified from spleens using an automated magnetic cell sorter (Auto MACS, Miltenyi Biotech, Germany) with >95% purity in all experiments. These cells (1×10^5) were stimulated for 48 h with MyHC-α peptides in the presence of irradiated (3000 cGy) splenocytes (5×10^5) from wild-type littermates. Cytokine levels in the culture supernatants were measured using ELISA kits (R&D Biosystems, USA) or the Bio-Plex suspension array system (BIO-RAD, USA). For proliferation assays, cells were pulsed with 2 μCi [^{3}H] thymidine for the last 12 h of culture.

2.5. In vitro Treg assays

$CD25^+CD4^+$ T-cells from wild-type or Sema4A-deficient mice were co-cultured with syngeneic $CD25^-CD4^+$T-cells (2×10^4) in the presence of irradiated (2000 cGy) APCs (5×10^4) and anti-CD3 (10 μg/ml, clone 145-2C11, eBioscience, USA) for 3 days in 96-well round-bottomed plates. Incorporation of [^{3}H] thymidine by proliferating lymphocytes during the last 14 h of the culture was measured.

2.6. Isolation of heart-infiltrating cells

Heart-infiltrating cells were isolated as described previously [19]. The heart was cannulated with a 22-gauge needle from the apex to the left ventricle after binding the ascending aorta. The heart was perfused at a constant flow of 1.1 ml/min for 3 min with a Ca^{2+}-free bicarbonate-based buffer as described previously [19]. Enzymatic digestion was initiated by perfusing with the above solution containing collagenase D (0.895 mg/ml, Roche, Switzerland) and protease type XIV (0.5 mg/ml, Sigma) for an additional 7 min. The heart was placed into a Petri

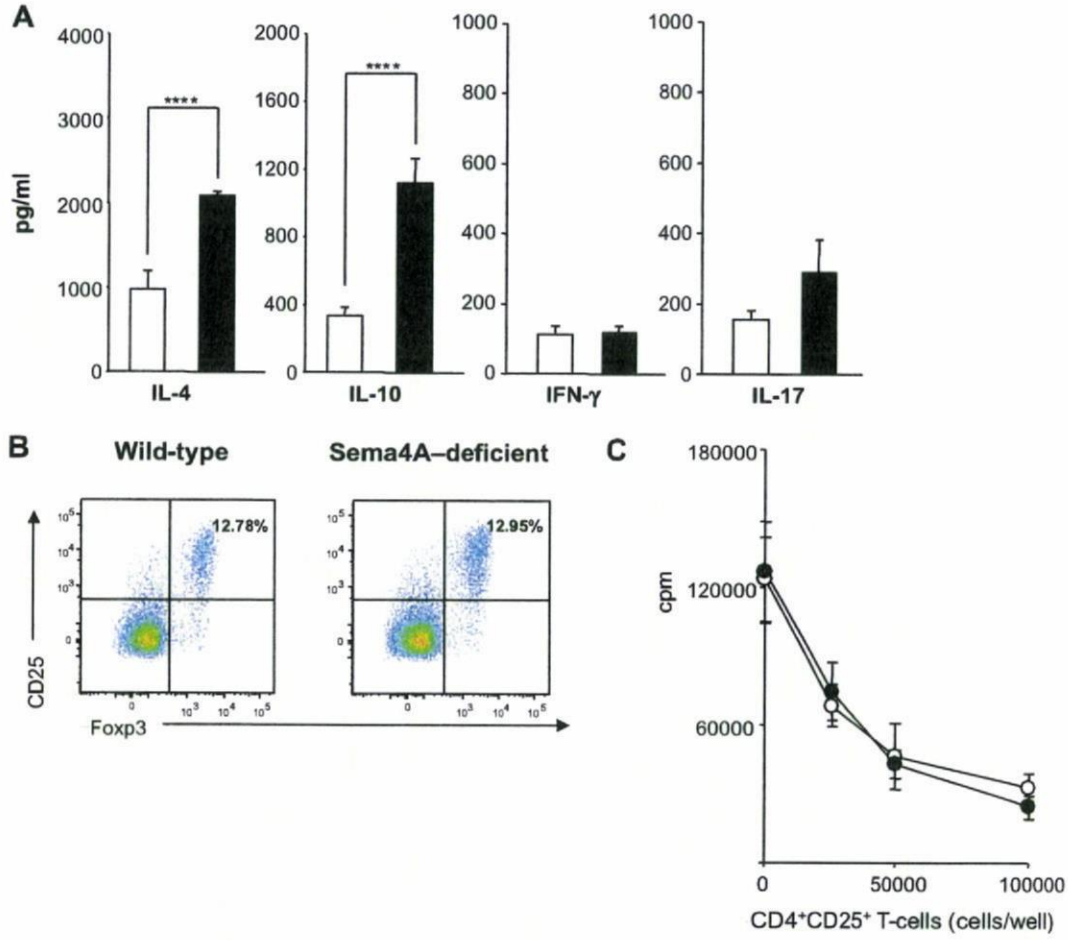

Fig. 2. $CD4^+$ T-cells from Sema4A-deficient mice produced high amounts of IL-4 and IL-10. (A) $CD4^+$ T-cell cytokine production patterns of immunized wild-type versus Sema4A-deficient mice. $CD4^+$ T-cells isolated from the spleens of immunized wild-type (white bars) or Sema4A-deficient mice (black bars) were restimulated with a MyHC-α peptide. The cytokine levels in the culture supernatants were measured by Bio-Plex after 48 h of restimulation. Error bars indicate means ± S.D. ****, $P < 0.001$; each value was analyzed by a student *t*-test. (B) $CD4^+$ T-cells isolated from the spleens of immunized wild-type or Sema4A-deficient mice were analyzed by intracellular staining. (C) Normal activities of Treg in Sema4A-deficient mice. $CD25^+CD4^+$ T-cells from wild-type (open circles) or Sema4A-deficient (closed circles) mice were co-cultured with syngeneic $CD25^-CD4^+$T-cells in the presence of irradiated APCs and anti-CD3 for 3 days. Incorporation of [^{3}H] thymidine by proliferating lymphocytes during the last 14 h of the culture was measured. Error bars indicate means ± S.D.

dish containing chilled staining buffer (2% fetal bovine serum, 0.05% sodium azide in phosphate-buffered saline) and manually dispersed into a single cell suspension using razor blades. Single cell suspensions were sequentially filtered through 100-μm and 40-μm cell strainers (BD Falcon, USA) and finally through 20-μm self-assembled strainers (Millipore, USA).

2.7. Adoptive T-cell transfers

Spleen cells from EAM mice were cultured for 72 h on MyHC-α (10 μg/ml)-pulsed irradiated splenocytes in the presence of an anti-CD28 monoclonal antibody (5 μg/ml clone 37.51 BD Pharmingen). $CD4^+$ T-cells were negatively sorted by autoMACS and transferred into recipient SCID mice (1×10^6 cells/mouse). Ten days after $CD4^+$ T-cell transfer, myocarditis was scored as described above.

2.8. Flow cytometry

Cells were stained with the following antibodies: anti-CD45 (Ly-5), anti-CD3 (145-2C11), anti-Gr-1 (RB6-8C5), anti-CD11b (M1/70) conjugated with FITC, phycoerythrin (PE) in the presence of Fc block (anti-CD16/32, 2.4G2). Analysis of intracellular forkhead box P3 (Foxp3) was performed according to the manufacturer's protocol (eBioscience). All antibodies were from eBiosciences, except for the anti-CD11b, which was purchased from BD Pharmingen.

3. Results and discussion

3.1. Sema4A-deficient mice were resistant to EAM

We previously found that Sema4A is crucial for the differentiation of $CD4^+$ T-cells [14]. To investigate the pathogenic relevance of Sema4A in the development of EAM, we injected MyHC-α-loaded DCs into Sema4A-deficient or wild-type mice and examined their hearts for inflammation. Wild-type mice exhibited strong cardiac inflammatory disease with a significant infiltration of inflammatory mononuclear cells (Fig. 1A). The hearts from wild-type mice were macroscopically enlarged (data not shown). In contrast, Sema4A-deficient mice showed a very mild phenotype (Fig. 1A and B). Consistent with the difference in the severities of EAM, the total number of infiltrating $CD45^+$ inflammatory cells was significantly decreased in Sema4A-deficient mice compared to wild-type mice (Fig. 1C). In addition, the proportions of infiltrating macrophages and granulocytes among infiltrating inflammatory cells in Sema4A-deficient mice were much lower than those in wild-type mice (Fig. 1C). Collectively, these findings strongly suggest that Sema4A is pathologically important for the development of EAM.

3.2. $CD4^+$ T-cells from Sema4A-deficient mice produced high amounts of IL-4 and IL-10

Sema4A plays a key role in differentiation of $CD4^+$ T-cells [14]. To investigate the relevance of Sema4A in T-cell activation in EAM, we performed T-cell recall assays. Consistent with previous findings on Sema4A-deficient mice [14], MyHC-α-specific T-cells showed significantly enhanced IL-4 and IL-10 production (Fig. 2A). Although it has been reported that IL-17 is involved in the development of EAM [20–22], IL-17 production by Sema4A-deficient T-cells was only slightly enhanced. In addition, in vitro T_H17 polarization of naïve Sema4A-deficient $CD4^+$ T-cells was not impaired (Supplementary Fig. 1A). These findings suggested that T_H17 was not involved in the resistance to EAM in Sema4A-deficient mice. To determine the involvement of regulatory T-cells (Treg), we performed intracellular Foxp3 staining of $CD4^+$ T-cells isolated from the spleens of EAM-induced mice. The proportion of $Foxp3^+$ Treg cells isolated from Sema4A-deficient mice was comparable to those from wild-type mice (Fig. 2B). Consistent with this finding, the suppressive activities of CD25+CD4+ T-cells were not affected in Sema4A-deficient mice (Fig. 2C) showing that Treg is not involved in the phenotype of Sema4A-deficient mice.

We have previously reported that Sema4A-deficient mice exhibited defective in vivo T_H1-responses but rather enhanced

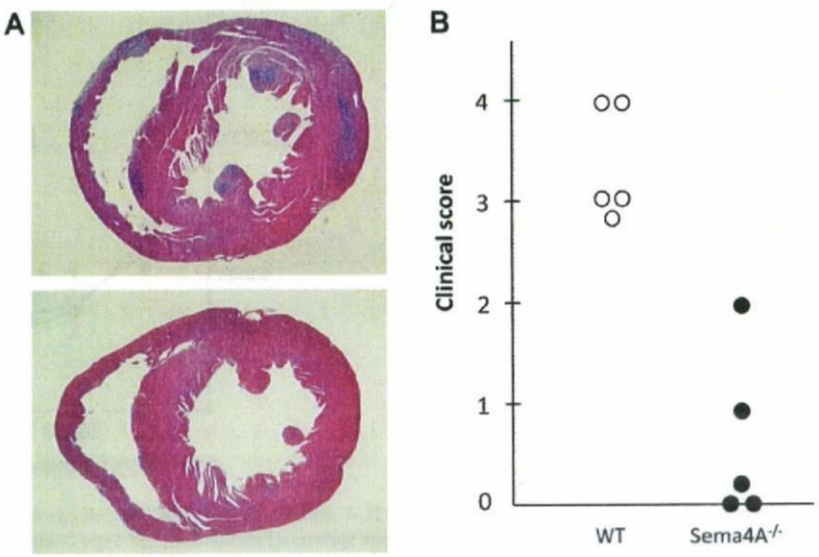

Fig. 3. $CD4^+$ T-cells from immunized Sema4A-deficient mice could not induce myocarditis. (A) Splenocytes from immunized wild-type or Sema4A-deficient mice were restimulated in vitro for 72 h with MyHC-α peptides and anti-CD28 antibodies. The resulting $CD4^+$ T-cells were purified and injected intraperitoneally into recipient SCID mice. $CD4^+$ T-cells from immunized wild-type mice (upper) but not Sema4A-deficient mice (lower) induced autoimmune myocarditis. (B) Disease severity scores of individual SCID mice with adoptively transferred $CD4^+$ T-cells from immunized wild-type (open circles) or Sema4A-deficient (closed circles) mice.

in vivo T_H2-responses [14]. Also in the case of the genetic defects in a Sema4A-receptor, Tim-2-deficient mice show exacerbated lung inflammation accompanied by enhanced T_H2-responses [23]. Consistent with this finding, we found that $CD4^+$ T-cells from Sema4A-deficient mice immunized with MyHC-α exhibited enhanced production of T_H2 cytokines, such as IL-4 and IL-10. In this context, the T_H2 bias in Sema4A-deficient mice seems to contribute to EAM resistance, although further studies would be required to determine how T_H2 cytokines are involved in this phenotype.

3.3. Abnormal $CD4^+$ T-cells were responsible for the resistance to myocarditis in Sema4A-deficient mice

To determine whether the abnormal differentiation of helper T-cells was responsible for the resistance to myocarditis in Sema4A-deficient mice, we isolated splenic T-cells from mice that had been immunized with DCs, stimulated these T-cells with MyHC-α presented by syngeneic antigen-presenting cells, and adoptively transferred these T-cells into SCID mice. As shown in Fig. 3A, wild-type $CD4^+$ T-cells induced severe myocarditis. In contrast, Sema4A-deficient $CD4^+$ T-cells did not induce myocarditis (Fig. 3B). However, Sema4A-deficient $CD4^+$ T-cells proliferated in response to MyHC-α-peptides to the same extent as wild-type $CD4^+$ T-cells (Supplementary Fig. 1B). Taken together, our results indicate that abnormal $CD4^+$ T-cell differentiation was primarily responsible for the resistance to EAM in Sema4A-deficient mice.

In summary, we demonstrated that Sema4A-deficient mice were resistant to the initiation of EAM, in which increased T_H2 cytokines production by Sema4A-deficient $CD4^+$ T-cells seems to be important for this resistance. Our findings suggest that Sema4A is critically involved in the development of myocarditis and dilated cardiomyopathy.

Acknowledgements: We thank T. Yazawa for technical support. This study was supported by research grants from the Ministry of Education, Culture, Sports, Science and Technology of Japan, the program for Promotion of Fundamental Studies in Health Sciences of the National Institute of Biomedical Innovation (A.K.), the Target Protein Research Program of the Japan Science and Technology Agency (T.T and A.K.), Uehara memorial foundation (A.K.) and Takeda Scientific Foundation (T.T. and A.K.).

Appendix A. Supplementary data

Supplementary data associated with this article can be found, in the online version, at doi:10.1016/j.febslet.2008.10.040.

References

[1] Feldman, A.M. and McNamara, D. (2000) Myocarditis. N. Engl. J. Med. 343, 1388–1398.
[2] Spotnitz, M.D. and Lesch, M. (2006) Idiopathic dilated cardiomyopathy as a late complication of healed viral (Coxsackie B virus) myocarditis: historical analysis, review of the literature, and a postulated unifying hypothesis. Prog. Cardiovasc. Dis. 49, 42–57.
[3] Kishimoto, C., Hiraoka, Y., Takamatsu, N., Takada, H., Kamiya, H. and Ochiai, H. (2003) An in vivo model of autoimmune post-coxsackievirus B3 myocarditis in severe combined immunodeficiency mouse. Cardiovasc. Res. 60, 397–403.
[4] Pummerer, C.L., Luze, K., Grassl, G., Bachmaier, K., Offner, F., Burrell, S.K., Lenz, D.M., Zamborelli, T.J., Penninger, J.M. and Neu, N. (1996) Identification of cardiac myosin peptides capable of inducing autoimmune myocarditis in BALB/c mice. J. Clin. Invest. 97, 2057–2062.
[5] Eriksson, U., Ricci, R., Hunziker, L., Kurrer, M.O., Oudit, G.Y., Watts, T.H., Sonderegger, I., Bachmaier, K., Kopf, M. and Penninger, J.M. (2003) Dendritic cell-induced autoimmune heart failure requires cooperation between adaptive and innate immunity. Nat. Med. 9, 1484–1490.
[6] Fuse, K., Kodama, M., Ito, M., Okura, Y., Kato, K., Hanawa, H., Aoki, S. and Aizawa, Y. (2003) Polarity of helper T cell subsets represents disease nature and clinical course of experimental autoimmune myocarditis in rats. Clin. Exp. Immunol. 134, 403–408.
[7] Dong, C. (2006) Diversification of T-helper-cell lineages: finding the family root of IL-17-producing cells. Nat. Rev. Immunol. 6, 329–333.
[8] Kaya, Z., Dohmen, K.M., Wang, Y., Schlichting, J., Afanasyeva, M., Leuschner, F. and Rose, N.R. (2002) Cutting edge: a critical role for IL-10 in induction of nasal tolerance in experimental autoimmune myocarditis. J. Immunol. 168, 1552–1556.
[9] Watanabe, K., Nakazawa, M., Fuse, K., Hanawa, H., Kodama, M., Aizawa, Y., Ohnuki, T., Gejyo, F., Maruyama, H. and Miyazaki, J. (2001) Protection against autoimmune myocarditis by gene transfer of interleukin-10 by electroporation. Circulation 104, 1098–1100.
[10] Cihakova, D., Barin, J.G., Afanasyeva, M., Kimura, M., Fairweather, D., Berg, M., Talor, M.V., Baldeviano, G.C., Frisancho, S., Gabrielson, K., Bedja, D. and Rose, N.R. (2008) Interleukin-13 protects against experimental autoimmune myocarditis by regulating macrophage differentiation. Am. J. Pathol. 172, 1195–1208.
[11] Pasterkamp, R.J. and Kolodkin, A.L. (2003) Semaphorin junction: making tracks toward neural connectivity. Curr. Opin. Neurobiol. 13, 79–89.
[12] Toyofuku, T., Zhang, H., Kumanogoh, A., Takegahara, N., Suto, F., Kamei, J., Aoki, K., Yabuki, M., Hori, M., Fujisawa, H. and Kikutani, H. (2004) Dual roles of Sema6D in cardiac morphogenesis through region-specific association of its receptor, Plexin-A1, with off-track and vascular endothelial growth factor receptor type 2. Genes Dev. 18, 435–447.
[13] Suzuki, K., Kumanogoh, A. and Kikutani, H. (2008) Semaphorins and their receptors in immune cell interactions. Nat. Immunol. 9, 17–23.
[14] Kumanogoh, A., Shikina, T., Suzuki, K., Uematsu, S., Yukawa, K., Kashiwamura, S., Tsutsui, H., Yamamoto, M., Takamatsu, H., Ko-Mitamura, E.P., Takegahara, N., Marukawa, S., Ishida, I., Morishita, H., Prasad, D.V., Tamura, M., Mizui, M., Toyofuku, T., Akira, S., Takeda, K., Okabe, M. and Kikutani, H. (2005) Nonredundant roles of Sema4A in the immune system: defective T cell priming and Th1/Th2 regulation in Sema4A-deficient mice. Immunity 22, 305–316.
[15] Kumanogoh, A., Marukawa, S., Suzuki, K., Takegahara, N., Watanabe, C., Ch'ng, E., Ishida, I., Fujimura, H., Sakoda, S., Yoshida, K. and Kikutani, H. (2002) Class IV semaphorin Sema4A enhances T-cell activation and interacts with Tim-2. Nature 419, 629–633.
[16] Kuchroo, V.K., Dardalhon, V., Xiao, S. and Anderson, A.C. (2008) New roles for TIM family members in immune regulation. Nat. Rev. Immunol. 8, 577–580.
[17] Inaba, K., Inaba, M., Romani, N., Aya, H., Deguchi, M., Ikehara, S., Muramatsu, S. and Steinman, R.M. (1992) Generation of large numbers of dendritic cells from mouse bone marrow cultures supplemented with granulocyte/macrophage colony-stimulating factor. J. Exp. Med. 176, 1693–1702.
[18] Marsland, B.J., Nembrini, C., Grun, K., Reissmann, R., Kurrer, M., Leipner, C. and Kopf, M. (2007) TLR ligands act directly upon T cells to restore proliferation in the absence of protein kinase C-theta signaling and promote autoimmune myocarditis. J. Immunol. 178, 3466–3473.
[19] Afanasyeva, M., Georgakopoulos, D., Belardi, D.F., Ramsundar, A.C., Barin, J.G., Kass, D.A. and Rose, N.R. (2004) Quantitative analysis of myocardial inflammation by flow cytometry in murine

autoimmune myocarditis: correlation with cardiac function. Am. J. Pathol. 164, 807–815.
[20] Rangachari, M., Mauermann, N., Marty, R.R., Dirnhofer, S., Kurrer, M.O., Komnenovic, V., Penninger, J.M. and Eriksson, U. (2006) T-bet negatively regulates autoimmune myocarditis by suppressing local production of interleukin 17. J. Exp. Med. 203, 2009–2019.
[21] Sonderegger, I., Rohn, T.A., Kurrer, M.O., Iezzi, G., Zou, Y., Kastelein, R.A., Bachmann, M.F. and Kopf, M. (2006) Neutralization of IL-17 by active vaccination inhibits IL-23-dependent autoimmune myocarditis. Eur. J. Immunol. 36, 2849–2856.
[22] Valaperti, A., Marty, R.R., Kania, G., Germano, D., Mauermann, N., Dirnhofer, S., Leimenstoll, B., Blyszczuk, P., Dong, C., Mueller, C., Hunziker, L. and Eriksson, U. (2008) CD11b+ monocytes abrogate Th17 CD4+ T cell-mediated experimental autoimmune myocarditis. J. Immunol. 180, 2686–2695.
[23] Rennert, P.D., Ichimura, T., Sizing, I.D., Bailly, V., Li, Z., Rennard, R., McCoon, P., Pablo, L., Miklasz, S., Tarilonte, L. and Bonventre, J.V. (2006) T cell, Ig domain, mucin domain-2 gene-deficient mice reveal a novel mechanism for the regulation of Th2 immune responses and airway inflammation. J. Immunol. 177, 4311–4321.

Developmental Biology 324 (2008) 1–9

Contents lists available at ScienceDirect

Developmental Biology

journal homepage: www.elsevier.com/developmentalbiology

Plexin A3 and plexin A4 convey semaphorin signals during facial nerve development

Quenten Schwarz [a], Kathryn E. Waimey [b], Matthew Golding [c], Hyota Takamatsu [d], Atsushi Kumanogoh [d], Hajime Fujisawa [e], Hwai-Jong Cheng [b], Christiana Ruhrberg [a,*]

[a] UCL Institute of Ophthalmology, University College London, 11-43 Bath Street, London EC1V 9EL, UK
[b] Center for Neuroscience, 1544 Newton Court, University of California, Davis, California 95618, USA
[c] Molecular Neuropathobiology Laboratory, Cancer Research UK London Research Institute, 44 Lincoln's Inn Fields, London WC2A 3PX, UK
[d] Department of Immunopathology, World Premier International Immunology Frontier Research Center and Research Institute for Microbial Diseases, Osaka University, 3-1 Yamada-oka, Suita, Osaka 565-0871, Japan
[e] Nagoya University Graduate School of Science, Chikusa-ku, Nagoya 464-8602, Japan

ARTICLE INFO

Article history:
Received for publication 4 May 2008
Revised 16 August 2008
Accepted 18 August 2008
Available online 3 September 2008

Keywords:
Facial nerve
Facial branchiomotor neuron
Facial visceromotor neuron
Greater superficial petrosal nerve
Axon guidance
Neuropilin
Plexin
Semaphorin
SEMA3A
SEMA3F

ABSTRACT

In vertebrates, class 3 semaphorins (SEMA3) control axon behaviour by binding to neuronal cell surface receptors composed of a ligand binding subunit termed neuropilin (NRP) and a signal transduction subunit of the A-type plexin family (PLXNA). We have determined the requirement for SEMA3/NRP/PLXN signalling in the development of the facial nerve, which contains axons from two motor neuron populations, branchiomotor and visceromotor neurons. Loss of either SEMA3A/NRP1 or SEMA3F/NRP2 caused defasciculation and ectopic projection of facial branchiomotor axons. In contrast, facial visceromotor axons selectively required SEMA3A/NRP1. Thus, the greater superficial petrosal nerve was defasciculated, formed ectopic projections and failed to branch in its target area when either SEMA3A or NRP1 were lost. To examine which A-type plexin conveyed SEMA3/neuropilin signals during facial nerve development, we combined an expression analysis with loss of function studies. Even though all four A-type plexins were expressed in embryonic motor neurons, PLXNA1 and PLXNA2 were not essential for facial nerve development. In contrast, loss of PLXNA4 phenocopied the defects of SEMA3A and NRP1 mutants, and loss of PLXNA3 phenocopied the defects of SEMA3F and NRP2 mutants. The combined loss of PLXNA3 and PLXNA4 impaired facial branchiomotor axon guidance more severely than loss of either plexin alone, suggesting that SEMA3A and SEMA3F signals, even though both essential, are partially redundant.

Introduction

The brainstem of the adult vertebrate brain contains several different types of motor neurons that control important physiological processes, for example feeding, speech and eye movement. These motor neurons can be classified into subtypes according to their synaptic targets and the projection pattern of their axons as they leave the brain. The axons of branchiomotor neurons innervate muscles within the branchial arches, whilst the axons of visceromotor neurons innervate parasympathetic ganglia and smooth muscles. The somatic motor neurons, on the other hand, innervate muscles derived from paraxial or prechordal mesoderm. As they leave the hindbrain, the axons of visceromotor and branchiomotor neurons converge on shared dorsal exit points, whereas the axons of most somatic motor neurons exit ventrally. The anatomical organisation and function of these brainstem nerves is set up during embryonic development, when hindbrain motor neurons develop in lineage-restricted compartments termed rhombomeres and express selective subsets of transcription factors to control the responsiveness of their axons to environmental guidance cues (reviewed by Cordes, 2001). Thus, axon migration within the hindbrain is governed by anteroposterior and dorsoventral cues that guide axons to defined exit points, whilst axon migration outside the hindbrain is controlled by repulsive cues that surround the nerve path in combination with attractive target-derived cues. In combination, these patterning mechanisms ensure that the axons of hindbrain motor neurons are wired appropriately to perform their adult functions. The identification of genes that control axonal patterning of the cranial nerves during embryogenesis therefore enhances our understanding of congenital abnormalities such as Duane syndrome and congenital facial nerve palsy, and in the future may also contribute to improved diagnosis of these conditions (reviewed by Traboulsi, 2007). In addition, the brainstem motor neurons present particularly good model systems to study the molecular mechanisms of axon guidance, as the anatomically well-defined arrangement of their cell bodies within the rhombomeres of the developing brain facilitates the identification of axon guidance receptors that are used by specific cranial motor nerves (Fig. 1B; see, for example, Auclair et al., 1996; Jacob and Guthrie, 2000; Lumsden and Keynes, 1989; Studer et al., 1996).

* Corresponding author. Fax: +44 207 608 6810.
E-mail address: c.ruhrberg@ucl.ac.uk (C. Ruhrberg).

0012-1606/$ – see front matter © 2008 Elsevier Inc. All rights reserved.
doi:10.1016/j.ydbio.2008.08.020

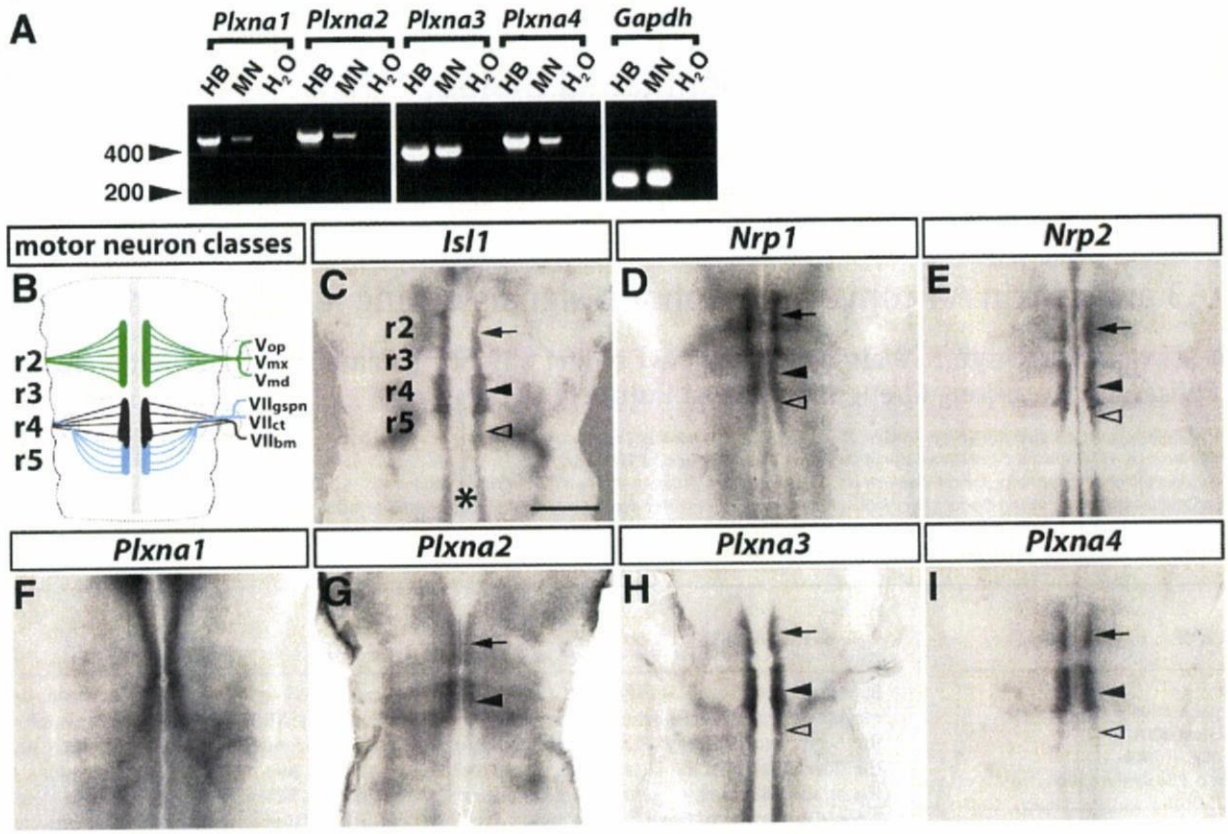

Fig. 1. A-type plexin expression in motor neurons. (A) RT-PCR analysis of mouse hindbrain tissue (HB), primary rat embryonic motor neurons (MN) and a negative control (H_2O) for *Plxna1-a4* and a *Gapdh* control; molecular weight marker: 200 and 400 bp (arrowheads). (B) Motor neuron populations in the mouse hindbrain at 10.5 dpc; r2-derived neurons are shown in green, r4-derived neurons in black and r5-derived neurons in blue; abbreviations: V_{op}, V_{max}, V_{md} – ophthalmic, maxillary and mandibular branches of the Vth cranial (trigeminal) nerve; VII_{gspn}, VII_{ct}, VII_{bm} – greater superficial petrosal nerve, chorda tympani and branchiomotor nerve of the VIIth cranial (facial) nerve. (C–I) Wholemount in situ hybridisation of 10.5 dpc mouse hindbrains. (C) A probe specific for the motor neuron marker *Isl1* reveals the nascent motor neuron column on each side of the midline (asterisk); focal thickenings at the level of r2 and r4 contain the trigeminal (arrow) and facial branchiomotor neurons (black arrowhead), respectively. Facial visceromotor neurons are born in r5 (clear arrowhead); r5 also contains caudally migrating facial branchiomotor neurons. (D, E) Hindbrain motor neurons express *Nrp1* (D) and *Nrp2* (E). *Plxna1* is expressed near the midline in all rhombomeres anterior to r5 (F); the expression patterns of *Plxna2* (G), *Plxna3* (H) and *Plxna4* (I) are consistent with a role in trigeminal (arrow) and facial (arrowhead) branchiomotor neurons; *Plxna3* (H) and *Plxna4* (I) are also expressed in posterior hindbrain motor neurons, including those in r5 (clear arrowhead). Scale bar (C–I): 500 μm.

The facial nerve contains axons from both branchiomotor and visceromotor neurons, which are born in two different rhombomeres (r) of the developing hindbrain. Whilst facial branchiomotor neurons are born in r4, facial visceromotor neurons are born in r5 (Figs. 1B, C; Auclair et al., 1996; Jacob and Guthrie, 2000; Lumsden and Keynes, 1989; Studer et al., 1996). Having left the hindbrain through a shared exit point in r4, their axons pass through the geniculate ganglion complex and then segregate again to innervate specific targets in the head and neck. The facial branchiomotor neurons (FBM) innervate the muscles of the second branchial arch, whereas the facial visceromotor neurons innervate the submandibular ganglion as the chorda tympani (CT) and the sphenopalatine ganglion as the greater superficial petrosal nerve (GSPN) (Fig. 1B).

The transmembrane protein neuropilin 1 (NRP1) is essential for the patterning of the facial nerve in the mouse, as it binds the secreted class 3 semaphorin SEMA3A to guide facial branchiomotor axons in the second branchial arch and the vascular endothelial growth factor isoform VEGF164 to control the position of facial branchiomotor neuron cell bodies within the hindbrain (Kitsukawa et al., 1997; Schwarz et al., 2004; Taniguchi et al., 1997). Mouse embryos lacking NRP1 or SEMA3A also show defasciculation of the trigeminal, glossopharyngeal and vagus cranial nerves (Kitsukawa et al., 1997; Taniguchi et al., 1997). Neuropilin 2 (NRP2) binds a different subset of class 3 semaphorins, and its principal ligand during axon guidance is SEMA3F (Chen et al., 1997). Loss of NRP2 or SEMA3F causes partial defasciculation of the facial branchiomotor and ophthalmic trigeminal nerves and severe defasciculation of the oculomotor nerve; in addition, the trochlear nerve fails to project to its target in these mutants (Chen et al., 2000; Giger et al., 2000; Sahay et al., 2003).

Neither NRP1 nor NRP2 are able to convey semaphorin signals on their own (Feiner et al., 1997). Rather, they recruit a member of the plexin family to control cytoskeletal behaviour in neurons (Rohm et al., 2000; Tamagnone et al., 1999). The neuropilins can associate with one of four different A-type plexins (PLXNA) in vitro (Rohm et al., 2000; Suto et al., 2003; Takahashi et al., 1999; Takahashi and Strittmatter, 2001; Tamagnone et al., 1999). However, targeted mouse mutations demonstrated plexin selectivity during semaphorin/neuropilin signalling in vivo. Thus, knockout studies did not confirm a direct role for PLXNA1 in sensory nerve axon guidance (Takegahara et al., 2006), even though truncated PLXNA1 protein blocks SEMA3A-induced growth cone turning in cultured sensory neurons (for example Rohm et al., 2000; Takahashi et al., 1999). Instead, specific combinations of the other three A-type plexins have been implicated in different axon guidance pathways both in vitro and in vivo (Bagri et al., 2003; Cheng et al., 2001; Palaisa and Granato, 2007; Suto et al., 2005; Tanaka et al., 2007; Waimey et al., 2008; Yaron et al., 2005). For example, PLXNA4 and, to a lesser extent, PLXNA3 are involved in the patterning of SEMA3A-responsive sensory and sympathetic axons, whilst PLXNA3, but not PLXNA4, is essential for the guidance of SEMA3F-responsive trochlear axons (Cheng et al., 2001; Suto et al., 2005; Yaron et al., 2005). In the mouse, PLXNA4 also cooperates with PLXNA2 to control the projection of hippocampal mossy fibres, but this mechanism depends

on the transmembrane semaphorin SEMA6A, rather than a secreted semaphorin (Suto et al., 2007). SEMA6A/PLXNA2 signalling also controls the migration of cerebellar granule cells (Renaud et al., 2008). In the chick, PLXNA1, PLXNA2 and PLXNA4 are all expressed in spinal motor neurons (Mauti et al., 2006), but the role of the A-type plexins in the development of hindbrain motor neurons has not yet been investigated. We now demonstrate that axonal patterning of facial branchiomotor and visceromotor neurons is differentially regulated by a specific combination of class 3 semaphorins and their neuropilin/plexin receptors. Our observations support the previously proposed concept of selective ligand/receptor pairings in semaphorin pathways. Moreover, they significantly advance our knowledge of facial nerve development, which is affected in several types of congenital human craniofacial syndromes.

Experimental procedures

Animals

To obtain mouse embryos of defined gestational ages, mice were mated in the evening, and the morning of vaginal plug formation was counted as 0.5 days *post coitum* (dpc). Mice lacking NRP1, NRP2, SEMA3A, SEMA3F, PLXNA1, PLXNA2, PLXNA3 or PLXNA4 have previously been described (Cheng et al., 2001; Giger et al., 2000; Gu et al., 2003; Kitsukawa et al., 1997; Sahay et al., 2003; Suto et al., 2005; Takegahara et al., 2006; Taniguchi et al., 1997; Yaron et al., 2005). Genotyping protocols can be supplied on request.

RT-PCR analysis of hindbrain tissue and isolated motor neurons

12.5 dpc mouse hindbrains were dissected in ice-cold PBS. Primary motor neurons were purified from dissected embryonic rat neural tubes (14.5 dpc, corresponding to 13.5 dpc in the mouse (Henderson et al., 1995). RNA was extracted with Tri Reagent (Helena BioSciences) and subjected to RT-PCR using Superscript II (Invitrogen) for cDNA synthesis. For PCR amplification, the following oligonucleotide pairs were used: *Nrp1* 5′-gttgctgtgcgccacgctcgcccttg-3′ and 5′-ctgaagaggagcggatccggccaggag-3′ (431 bp); *Gapdh* 5′-gctgagtatgtcgtggagtc-3′ and 5′-ttggtggtgcaggatgcatt-3′ (192 bp); *Plxna1* 5′-tctagattctggtggaccttgcaaac-3′ and 5′-tctagaaggtgagtggcaatggatg (488 bp); *Plxna2* 5′-tccactctgagaatcgtgac-3′ and 5′-gagctcatagtccagcattg-3′ (530 bp); *Plxna3* 5′-gtgaacaagctgctcctcatag-3′ and 5′-gtgtctgaagggatcttgatc-3′ (358 bp); *Plxna4* 5′-tgtacacctcaaagcttgtg-3′ and 5′-gtccctgtcttctgtgaaga-3′ (467 bp).

Immunolabelling

Mouse embryos were fixed in ice-cold Dent's fixative (four parts methanol, 1 part dimethylsulfoxide) and incubated in Dent's fixative containing 10% hydrogen peroxide for 2 h to quench endogenous peroxidase activity. Samples were washed several times in TBS (10 mM Tris–HCl pH8.0 and 150 mM NaCl), incubated for 30 min in blocking solution (normal goat serum containing 20% DMSO and 0.12% thimerosal; Sigma) and incubated over night in blocking solution that contained rabbit anti neurofilament antibodies (Chemicon). After several washes in TBS, samples were incubated over night in blocking solution containing horseradish peroxidase-conjugated goat anti rabbit IgG (DAKO). After washing, peroxidase activity was detected with diaminobenzidine and hydrogen peroxide (SigmaFast; Sigma). Stained samples were fixed in formaldehyde and then dehydrated in methanol. Samples were then cleared in a solution containing 2 parts benzyl benzoate and 1 part benzyl alcohol. Images were recorded using the MZ16 microscope (Leica) equipped with a ProgResC14 digital camera (Jenoptiks). In some experiments, the neurofilament antibody was detected with Alexa488-conjugated goat anti rabbit IgG (Molecular Probes) and images were then recorded using an Olympus SZX16 fluorescent stereomicroscope equipped with an ORCA-HR digital camera (Hamamatsu Photonics). Images were processed using Openlab 2.2 software (Improvision Ltd.) and Adobe Photoshop 7.0 (Adobe Systems, Inc.).

In situ hybridisation

For in situ hybridisation, embryos were fixed over night in 4% formaldehyde in phosphate buffered saline (PBS), washed in PBS, dehydrated in methanol and stored at −20 °C. In situ hybridization was performed according to a previously published method (Riddle et al., 1993) using digoxigenin-labelled riboprobes transcribed from plasmids containing the following cDNAs: *Sema3a* and *Sema3f* (gift from M. Tessier-Lavigne), *Isl1* (gifts of T. Jessell, Columbia University, New York), *Nrp1* (gift from M. Fruttiger, University College London) and *Phox2b* (gift from C. Goridis, INSERM, Marseille, France). Riboprobes for A-type plexins were transcribed from expressed sequence tag (EST) IMAGE clones (Invitrogen), clone IDs: 791967 (*Plxna1*), 5364824 (*Plxna2*), 401253 (*Plxna3*) and 4316766 (*Plxna4*). Images were acquired as described above.

DiI labelling of facial visceromotor neurons

11.0 dpc wild type embryos were fixed over night in 4% formaldehyde in PBS. DiI crystals (Invitrogen) were then placed into small incisions of dorsal r5 hindbrain tissue. DiI-labelled embryos were incubated in PBS with 0.02% sodium azide at 37 °C in the dark for 9 days. The lower jaw was removed for photography. Images were recorded with the SZX16 dissecting microscope as described above.

Results

Expression pattern of A-type plexins during hindbrain development

To determine which plexins are expressed in developing motor neurons, we initially analysed rat embryo primary motor neurons by RT-PCR and detected expression of all 4 A-type plexins (Fig. 1A). We then compared the expression pattern of these plexins to that of the motor neuron marker *Isl1* (Fig. 1C) and the plexin co-receptors *Nrp1* (Fig. 1D) and *Nrp2* (Fig. 1E) in mouse hindbrains at 10.5 dpc, when cranial motor neurons extend axons through their hindbrain exit points into the periphery. *Plxna1* was expressed near the midline in all rhombomeres anterior to r5, but its pattern was not consistent with specific expression in facial branchiomotor or visceromotor neurons (compare Fig. 1C with F). In contrast, the patterns of *Plxna2* (Fig. 1G), *Plxna3* (Fig. 1H) and *Plxna4* (Fig. 1I) were consistent with expression by trigeminal and facial branchiomotor neurons; in addition, *Plxna3* and *Plxna4* were expressed in the r5 motor column, where facial visceromotor neurons originate, and in posterior hindbrain motor neurons (Figs. 1H, I). In summary, the expression patterns suggested that all four plexins play a role in hindbrain development, with PLXNA3 and PLXNA4 being the best candidate mediators of facial motor neuron patterning.

PLXNA3 and PLXNA4 convey semaphorin signals to guide facial branchiomotor axons

To determine the functional requirement for the A-type plexins in facial nerve development, we examined axonal patterning in the corresponding loss of function mouse mutants. We found that loss of PLXNA1 or PLXNA2 did not obviously impair axon guidance or fasciculation of the facial or trigeminal nerves (compare Fig. 2A with D, G; 3/3 cases). In contrast, loss of PLXNA3 or PLXNA4 caused defasciculation of the facial branchiomotor nerve (white arrowheads in Figs. 2H, I; 3/3 and 4/4 cases, respectively). Loss of either plexin also caused defasciculation of the ophthalmic branch of the

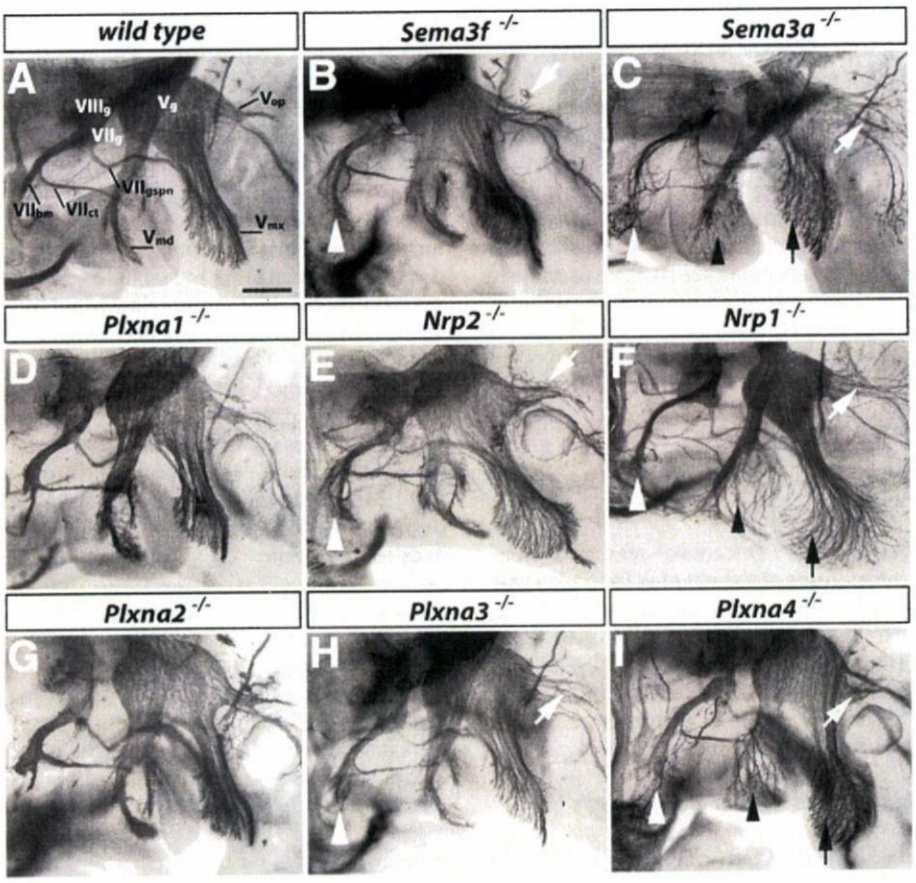

Fig. 2. PLXNA3 and PLXNA4 convey semaphorin signals during axon guidance of facial branchiomotor neurons. Wholemount neurofilament staining of 11.5 dpc wild type (A) and mutant embryos (B–I): a lateral view of the cranial nerves V (trigeminal) and VII (facial) is shown. The facial nerve segregates into 3 branches to form the facial branchiomotor nerve (VII_{bm}), the chorda tympani (VII_{ct}) and the greater superficial petrosal nerve (VII_{gspn}). The trigeminal nerve is also organised into 3 main branches: the mandibular (V_{md}), maxillary (V_{mx}), and ophthalmic (V_{op}) nerves. The facial (VII_g), vestibuloacoustic ($VIII_g$) and trigeminal (V_g) ganglia are indicated. Loss of PLXNA1 (D) or PLXNA2 (G) did not impair axon guidance of these nerves. Loss of SEMA3F (B), NRP2 (E) or PLXNA3 (H) caused defects in the VII_{bm} (white arrowhead) and V_{op} (white arrows). Loss of SEMA3A (C), NRP1 (F) or PLXNA4 (I) also caused VII_{bm} and V_{op} defects, with the VII_{bm} defects being more severe than in mutants lacking SEMA3F, NRP2 or PLXNA3. Note that the V_{op} defect was mild in the particular *Plxna4*-null mutant shown, but was stronger in other cases. Loss of SEMA3A, NRP1 or PLXNA4 also caused prominent defasciculation of the mandibular (black arrows) and maxillary (black arrowheads) nerves (C, F, I). Scale bar: 250 μm.

trigeminal nerve (white arrows in Figs. 2H, I; see Cheng et al., 2001; Yaron et al. 2005); however, the severity was variable between mutants of each genotype (data not shown). Interestingly, the maxillary and mandibular branches of the trigeminal nerve were defasciculated in *Plxna4*-null mutants (black arrows and arrowheads in 2I), but were not obviously affected in *Plxna3*-null mutants (compare Fig. 2A with H).

Consistent with the idea that PLXNA3 preferentially associates with NRP2 to form the SEMA3F receptor (Yaron et al., 2005), mutants lacking SEMA3F or NRP2 were similar to mutants lacking PLXNA3, displaying defasciculation of the facial branchiomotor and ophthalmic trigeminal branch, but not maxillary or mandibular trigeminal branches (compare Fig. 2H with B, E). On the other hand, mutants lacking NRP1 or SEMA3A were more similar to those lacking PLXNA4, with defasciculation of the facial branchiomotor nerve and the ophthalmic trigeminal branch, as well as the mandibular and maxillary trigeminal branches (compare Fig. 2I with C, F).

Semaphorin expression during axon guidance of facial visceromotor neurons

To examine if semaphorin-signalling through NRP/PLXN complexes also guides the visceromotor component of the facial nerve, we first characterised the axonal path of the greater superficial petrosal nerve (GSPN). Between 10.5 and 12.5 dpc, GSPN axons extend from the hindbrain through the facioacoustic ganglion (Fig. 2A) and then anteriorly, towards the site where the sphenopalatine ganglion forms (Figs. 3A–C). Anterograde DiI injection into the r5-derived hindbrain region, which gives rise to the facial visceromotor neurons, confirmed that these axons were indeed extended by facial visceromotor neurons (compare Fig. 3A with B).

Using *Phox2b* as a marker, it was previously reported that sphenopalatine ganglion neurons differentiate from 11.5 dpc onwards and begin to form a ganglion at 12.0 dpc (Enomoto et al., 2001). Consistent with this observation, we identified the anlagen of the sphenopalatine ganglion at 12.5 dpc in wholemounts (circled in Fig. 3F) and found that the ganglia were well established by 13.5 dpc (see below, Fig. 5A). By 12.5 dpc, the GSPN nerve had arborated in the area where the ganglion formed (compare Fig. 3C with F), presumably to establish contact with neurons in the sphenopalatine ganglion. Axon arborisation was present in most wild type embryos already at 11.5 dpc (Fig. 4A). In 11.0 dpc embryos, GSPN axons had reached the target field, but had not yet arborised (Fig. 3B). Taken together, these observations suggest that synaptic contact between presynaptic and postsynaptic sphenopalatine neurons is initiated between 11.25 and 11.5 dpc.

Sema3a and *Sema3f* were both expressed in regions surrounding the path of GSPN axons. Firstly, they were expressed bilaterally in an area flanking the axons as they extended towards the midline of the stomadeum (black arrows in Figs. 3D, E). This expression pattern was consistent with their general role as repellent cues that channel growing axons into fascicles. Secondly, both semaphorins were ex-

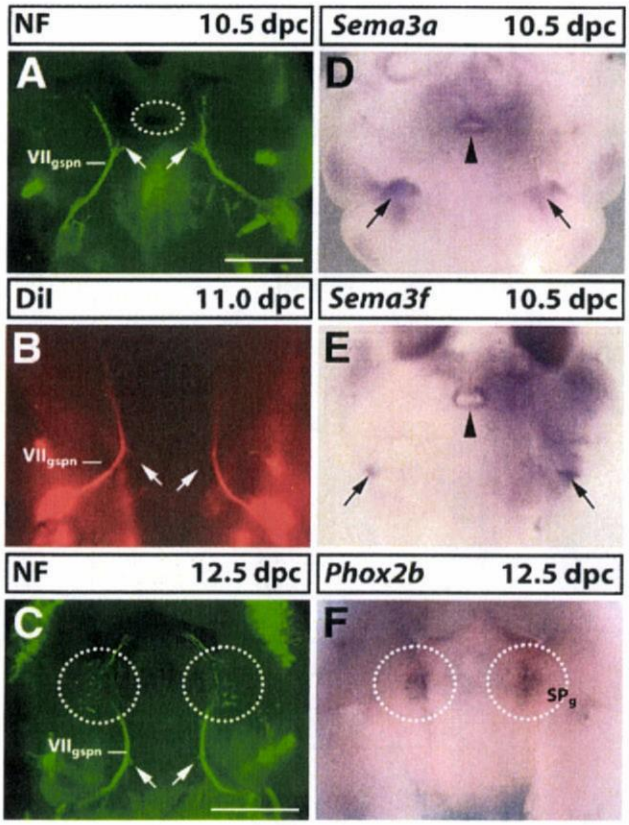

Fig. 3. Semaphorin expression during facial visceromotor axon guidance. (A–C) Wholemount visualisation of the GSPN nerve (VII_{gspn}) by neurofilament immunofluorescence (A, C) or anterograde DiI labelling (B) at 10.5 (A), 11.0 (B) or 12.5 dpc (C); ventral view, anterior up. The lower jaw including the trigeminal nerve branches was removed to afford better visualisation of the VII_{gspn}. At 10.5 dpc, VII_{gspn} axons extended from the main nerve trunk (arrows in panel A) towards Rathke's pouch (circled in panel A), but these axons had retracted by 11.0 dpc (arrows in panel B) and 12.5 dpc (arrows in panel C). (D, E) Wholemount in situ hybridisation at 10.5 dpc for *Sema3a* (D) and *Sema3f* (E) and at 12.5 dpc for the sphenopalatine ganglion (SP_g) marker *Phox2b* (F). The VII_{gspn} encounters two areas of high semaphorin expression as it extends towards its target site, one in the second pharyngeal arch (arrows in panels D, E) and one surrounding Rathke's pouch (arrowheads in panels D, E). At 12.5 dpc, VII_{gspn} axons arborated in the area where the SP_g had formed (compare circled areas in panel C with panel F). Scale bars: (A–E) and (C, F) 500 μm.

pressed around the opening of Rathke's pouch, which is located between the paired GSPN branches in the roof of the stomadeum (black arrowheads in Figs. 3D, E). This expression pattern was consistent with a role in repelling axons from the midline region; in agreement with this idea, short axon branches, which extended from each nerve towards the midline at 10.5 dpc, had retracted by 12.5 dpc (compare white arrows in Fig. 3A with C).

PLXNA4 conveys SEMA3A/NRP1 signals to guide facial visceromotor neurons

To test the hypothesis that NRP/PLXN signalling was essential for the guidance of facial visceromotor axons, we examined the behaviour of GSPN axons in loss of function mutants at 11.5 dpc by wholemount neurofilament staining (Fig. 4). Whilst axons formed normal projections in 5/5 *Nrp2*-null and 3/3 *Sema3F*-null mutants (compare Fig. 4A with B, E), we observed striking axon guidance errors in 5/5 *Nrp1*-null and 5/5 *Sema3a*-null mutants (Figs. 4C, F). Specifically, there was defasciculation (arrows in Figs. 4C, F) and midline crossing of ectopic axons (arrowheads in Figs. 4C, F) near Rathke's pouch, consistent with the idea that *Sema3a* normally provides repulsive cues for GSPN axons (see Fig. 3D). Moreover, there was no arborisation in the area where the sphenopalatine ganglion forms; rather, some axons appeared to extend beyond the target area (compare Fig. 4A with Figs. 4C, F).

We next examined which plexin transduced SEMA3A/NRP1 signals in facial visceromotor neurons. In PLXNA1 and PLXNA2 mutants, only the GSPN branch in the faster developing left side of the embryo had begun to arborate in the target area at 11.5 dpc, but axon pathfinding appeared intact (Figs. 4D, G); this observation is consistent with an overall developmental delay rather than a specific defect in axon guidance. In agreement with the idea that SEMA3F and NRP2 were not required for axon guidance of the GSPN, loss of PLXNA3 did not impair the pathfinding of the GSPN nerve (Fig. 4H). Instead, the defects of SEMA3A/NRP1 mutants were phenocopied by mutants lacking PLXNA4 (compare areas indicated by arrows and arrowheads in Figs. 4C, F with I). Taken together, the observations described in Figs. 3 and 4 suggest that SEMA3A signals through NRP1/PLXNA4 to guide visceromotor axons towards the site of sphenopalatine ganglion formation, preventing midline crossing and promoting target innervation.

Defects in visceromotor axon guidance occur in the presence of the sphenopalatine ganglion

It has been proposed that the sphenopalatine ganglion is essential for the pathfinding of GSPN axons from the facial ganglion to the target area (Jacob et al., 2000). We therefore asked if these pathfinding errors were secondary to loss of the sphenopalatine ganglion. This was also an important question, as the sphenopalatine ganglion is formed from r4-derived neural crest cells, and at least one subpopulation of r4-derived neural crest cells, which contributes to sensory gangliogenesis, migrates abnormally in *Sema3a*- and *Nrp1*-null mutants (Schwarz et al., 2008). We found that the paired sphenopalatine ganglia, even though mildly misshapen, were present in 4/4 *Nrp1*-null mutant embryos at 13.5 dpc (compare Fig. 5A with B). Nevertheless, the axonal trajectory of the GSPN was grossly abnormal in all those cases (compare Fig. 5C with D). We conclude that the pathfinding errors of visceromotor axons in mutants lacking SEMA3A, NRP1 or PLXNA4 are not due to loss of the target ganglion.

PLXNA3 and PLXNA4 cooperate during facial nerve development

The observations described above suggest that PLXNA3 and PLXNA4 independently transmit semaphorin signals to guide facial and trigeminal axons. Consistent with this idea, the facial branchiomotor nerve and all trigeminal nerve branches were more severely mispatterned in double knockouts than in single mutants (compare Fig. 6B with 4H, I; 6/6 cases). On the other hand, the facial visceromotor defects of double knockouts were not more severe than those of single *Plxna4* mutants (compare Fig. 6D with 4I; 4/4 cases). This observation is in agreement with the finding that PLXNA3 is not required for the patterning of this facial nerve branch (see Fig. 4). Therefore, PLXNA3 and PLXNA4 synergise to pattern the facial nerve, whereby both are required in branchiomotor neurons, but only PLXNA4 is essential in visceromotor neurons.

Discussion

Essential roles for class 3 semaphorins and their receptors in facial branchiomotor axon guidance

We have previously shown that SEMA3A signalling through NRP1 patterns the axons of facial branchiomotor neurons in the second branchial arch, affecting their pathfinding and fasciculation (Schwarz et al., 2004). We now show that SEMA3F and NRP2 also contribute to the patterning of facial branchiomotor neurons, because loss of either molecule results in similar axonal defects as loss of SEMA3A or NRP1 (Fig. 2). Our observation that one type of neuron can respond to two

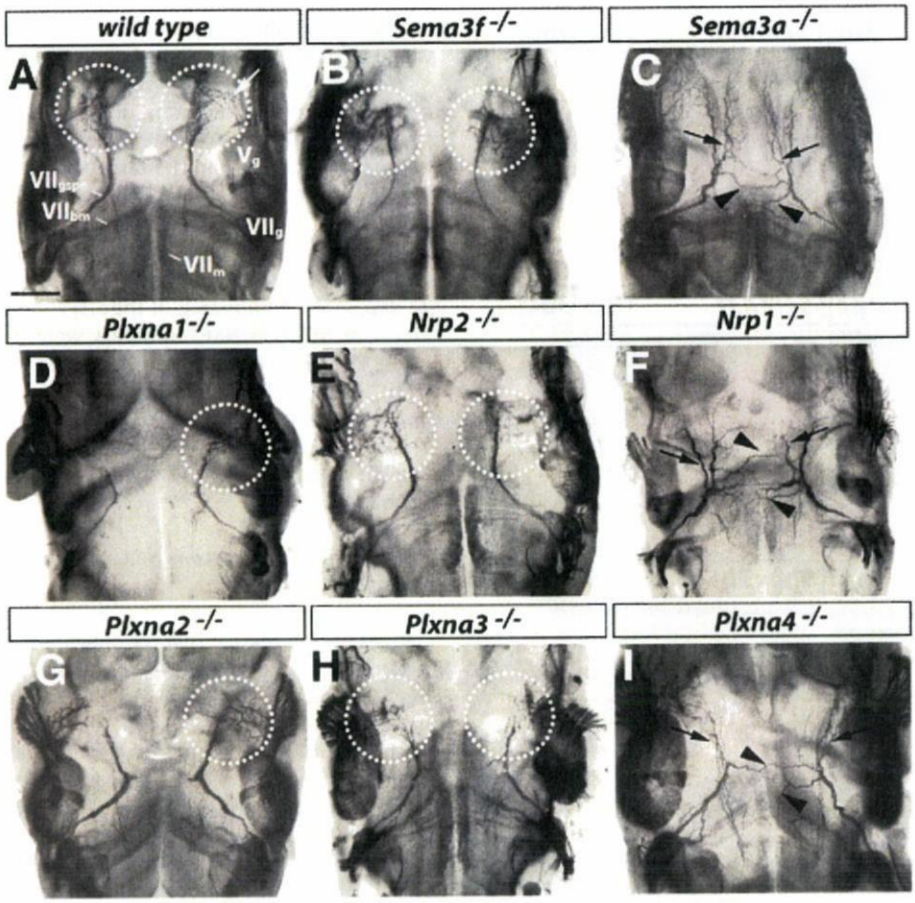

Fig. 4. SEMA3A signals through NRP1 and PLXNA4 to guide the axons of facial visceromotor neurons. (A) Wholemount neurofilament staining of wild type mouse embryos at 11.5 dpc reveals migrating facial branchiomotor neurons (VII_m), and their axons within the hindbrain, as well as the facioacoustic (VII_g) and trigeminal ganglia (V_g) and the greater superficial petrosal nerve (VII_{gspn}) in the periphery. VII_{gspn} axons arborate in the area where the sphenopalatine ganglion forms (circled); the white arrow denotes trigeminal axons that innervate the sphenopalatine ganglion. The lower jaw was removed to afford better visualisation of VII_{gspn} axons. (B–I) Corresponding wholemount neurofilament staining of loss of function mutants. Loss of SEMA3F (B) or NRP2 (E) did not affect VII_{gspn} axons. Similarly, loss of PLXNA1 (D), PLXNA2 (G) or PLXNA3 (H) did not impair their guidance. In contrast, loss of SEMA3A (C), NRP1 (F) or PLXNA4 (I) caused defasciculation (arrows) and midline crossing (arrowheads) of VII_{gspn} axons; moreover, there was no arborisation in the area where the sphenopalatine ganglion forms (compare panel A with panels C, F, I). Scale bar: 250 μm.

different semaphorins is consistent with the previous finding that hippocampal neurons respond two both SEMA3A and SEMA3F under physiological circumstances (Chedotal et al., 1998). Two different plexins were essential to transduce SEMA3A/NRP1 and SEMA3F/NRP2 signals, PLXNA3 and PLXNA4 (Fig. 2). These findings are consistent with previous observations in other model systems of axon guidance, which showed that PLXNA3 and PLXNA4 preferentially mediate SEMA3F and SEMA3A signals, respectively (Yaron et al., 2005).

PLXNA1 and PLXNA2 were also expressed in the hindbrain at the time of motor neuron differentiation, but their loss did not impair fasciculation or path finding of facial branchiomotor axons. We did, however, observe a delay in GSPN and trigeminal nerve branching in the area where the sphenopalatine ganglion forms (Fig. 4). Because this delay was not seen in *Nrp1*- or *Nrp2*-null mutants, it did not reflect a cell-autonomous defect in the neuropilin-mediated guidance of motor axons. Instead, it is likely an indirect consequence of an overall developmental delay or a defect in the nerve environment. Consistent with the latter possibility, PLXNA1 has been implicated as a SEMA6A-receptor in boundary cap patterning at the interface between the central and peripheral nervous systems to assist the ordered exit of axons form the neural tube (Mauti et al., 2007). It would also be interesting to examine if PLXNA1 and PLXNA2 play a role in SEMA3F-guided patterning events, for which PLXNA3 and PLXNA4 are dispensable, for example the guidance of trunk neural crest cells (Waimey et al., 2008).

In many model systems, SEMA3A acts as an environmental repellent for growing axons (for example, Luo et al., 1993; Messersmith et al., 1995). In addition, SEMA3A expression by motor neurons in the chick was previously shown to desensitise axons as they approach their target field (Moret et al., 2007). SEMA3A and SEMA3F are both expressed in the second pharyngeal arch from 8.5 dpc onwards, prior to the extension of motor axons out of the hindbrain (Schwarz et al., 2008). This observation is consistent with a model in which axon patterning is achieved by repulsive guidance cues in the environment. At subsequent developmental stages, SEMA3A is also expressed by the facial branchiomotor neurons themselves (Schwarz et al., 2004). Therefore, both paracrine and autocrine SEMA signalling through NRP/PLXN complexes may contribute to axon patterning of facial branchiomotor neurons, but these possibilities cannot be addressed with existing mouse models.

Target-independent guidance of facial visceromotor axons by SEMA3A signalling through NRP1/PLXNA4 receptors

In the vertebrate trunk, preganglionic and postganglionic sympathetic axons pathfind in the absence of their target, suggesting that guidance cues for sympathetic axons are derived from sources other than their target ganglia (for example, Guidry and Landis, 1995; Yip, 1987). Whilst parasympathetic neurons share transcription factors with sympathetic neurons to control their differentiation and have similar trophic requirements (reviewed in Jacob et al., 2000), it is not

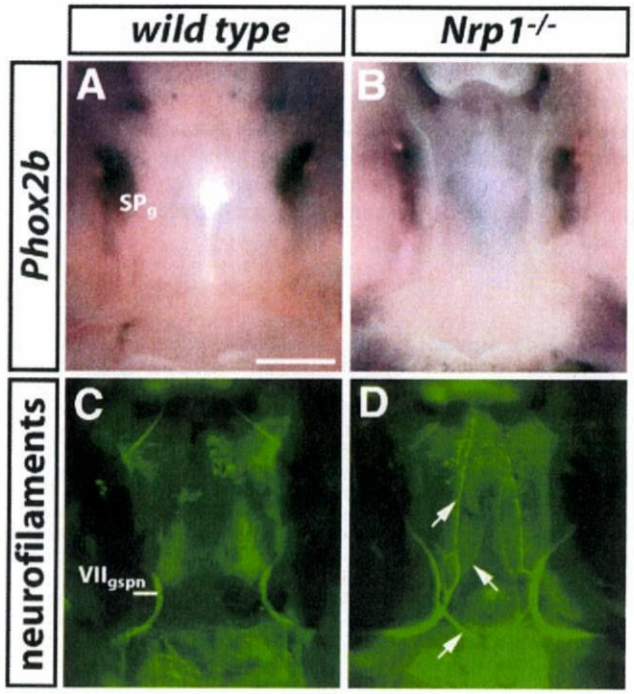

Fig. 5. Facial visceromotor axon guidance defects in the absence of SEMA3A/NRP1 signalling are not due to loss of the target ganglion. (A, B) Wholemount in situ hybridisation with a probe specific for Phox2b identifies the sphenopalatine ganglion (SP_g) in wild type (A) and *Nrp1*-null mutant (B) littermates at 13.5 dpc (ventral view). (C, D) Wholemount neurofilament staining of the developing palate of the same samples after in situ hybridisation shows an abnormal trajectory of the VII_{gspn} in the *Nrp1*-null mutant embryo (aberrant axons indicated with arrows in panel D). Note that the alkaline phosphatase reaction product, which was deposited during in situ hybridisation, partially obscured the VII_{gspn}. Scale bar (A–D): 500 μm.

clear if parasympathetic axons use guidance mechanisms that are similar to those of sympathetic axons.

A previous study using a loss of function mutant for the transcription factor *Phox2a* raised the possibility that facial visceromotor, unlike sympathetic axons, use a target-dependent mechanism of axon guidance, in which the sphenopalatine ganglion plays an essential role (Jacob et al., 2000). Specifically, the sphenopalatine ganglion was absent in these mutants, and this was accompanied by loss of the GSPN. However, these studies were complicated by the fact that *Phox2a* is not only essential for the formation of the sphenopalatine ganglion, but also for the formation of the geniculate ganglion (Jacob and Guthrie, 2000; Morin et al., 1997), which provides an intermediate target for facial visceromotor neurons en route from the hindbrain to the sphenopalatine ganglion. Moreover, *Phox2a* is expressed by all hindbrain motor neurons (Tiveron et al., 1996), including facial visceromotor neurons (Jacob et al., 2000). This observation raises the possibility that *Phox2a* contributes to visceromotor patterning in additional mechanisms that do not involve signals from the sphenopalatine ganglion. For example, the geniculate ganglion may be critical for pathfinding of facial visceromotor axons. Alternatively, *Phox2a* might control the expression of receptors in facial visceromotor neurons that are critical for nerve survival after axons have reached their target ganglion. This possibility was not addressed in the previous study, as the analysis of the GSPN was performed at 13.5 dpc, well after the axons of this nerve had reached the sphenopalatine ganglion in wild type mice and were likely to have made synaptic contact (see Figs. 3, 4).

We now demonstrate that facial visceromotor axons home in on their target area between 10.5 and 11.5 dpc, before the sphenopalatine ganglion is formed at 12.5 dpc (Figs. 3, 4). Moreover, we show that loss of SEMA3A signalling through NRP1/PLXNA4 impairs axon pathfinding at 11.5 dpc, i. e. before the sphenopalatine ganglion has formed (Figs. 4, 5). Finally, pathfinding errors in *Nrp1*-null mutants cannot be explained by loss of the geniculate ganglion, as it forms in embryos

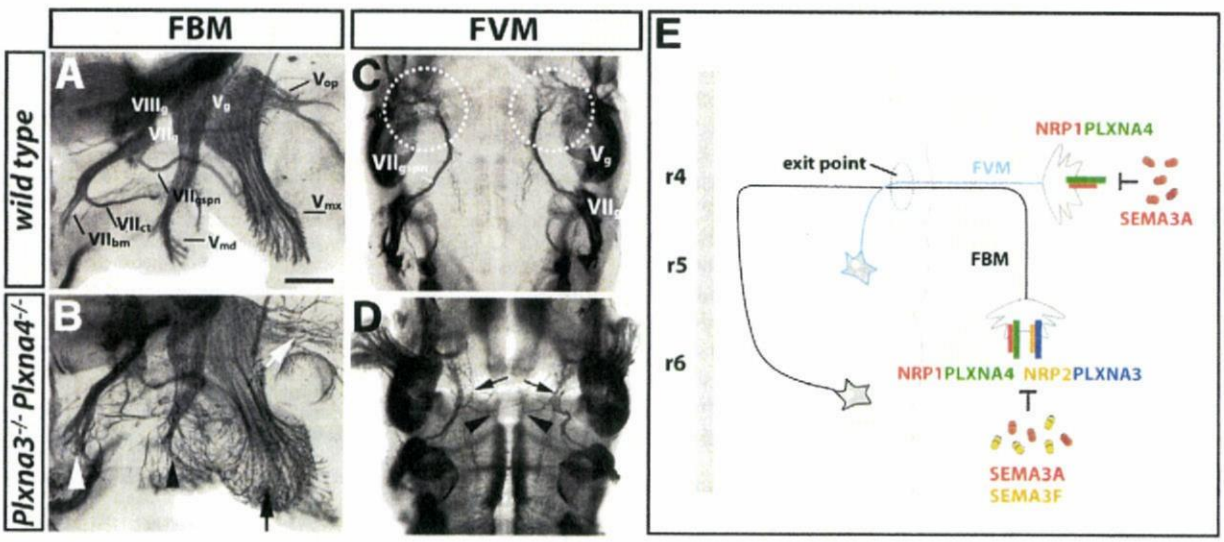

Fig. 6. PLXNA3 and PLXNA4 cooperation during facial branchiomotor, but not visceromotor axon guidance. (A–D) Wholemount neurofilament staining of wild type (A, C) and *Plxna3/Plxna4* double null mutants (B, D) at 11.5 dpc reveals the vestibuloacoustic ($VIII_g$), facial (VII_g) and trigeminal ganglia (V_g) as well as the three main facial and trigeminal nerve branches. (A, B) A lateral view of the head in a wild type shows the three facial branches, the branchiomotor nerve (VII_{bm}), the chorda tympani (VII_{ct}) and the greater superficial petrosal nerve (VII_{gspn}), as well the mandibular (V_{md}), maxillary (V_{mx}), and ophthalmic (V_{op}) branches of the trigeminal nerve. (B) The combined loss of PLXNA3 and PLXNA4 disrupted the patterning of the facial branchiomotor nerve (white arrowhead) as well as the mandibular (black arrowhead), maxillary (black arrow) and ophthalmic (white arrow) trigeminal nerve branches more severely than loss of either plexin alone (compare panel B with Figs. 2H, I). (C) A ventral view shows that VII_{gspn} axons normally arborate in the area where the sphenopalatine ganglion forms (circled). (D) The combined loss of PLXNA3 and PLXNA4 caused defasciculation (arrows) and midline crossing (arrowheads) of VII_{gspn} axons, and there was no arborisation in the area where the sphenopalatine ganglion forms; however, defects were not worse than those caused by loss of PLXNA4 alone (compare panel D with Fig. 4I). Scale bar (A–D) 250 μm. (E) Working model for facial nerve patterning: SEMA3A and SEMA3F cooperate to pattern facial branchiomotor neuron (FBM) axons by binding to NRP1/PLXNA4 and NRP2/PLXNA3, respectively; SEMA3A also patterns facial visceromotor neuron (FVM) axons by binding to NRP1/PLXNA4 complexes.

lacking NRP1 (Schwarz et al., 2008). Taken together, our observations suggest that preganglionic parasympathetic axons use target-independent mechanisms of axon guidance to approach their target field, and that the parasympathetic ganglia are more likely to play a role during subsequent stages of visceromotor axon patterning, perhaps by inducing axon arborisation or stimulating survival pathways.

Differential use of plexins during axon guidance of facial nerve subdivisions

All A-type plexins have been implicated as signal transducers for neuropilin-bound semaphorin signals during axon guidance in vitro. Initially, truncated PLXNA1 protein was shown to block SEMA3A-induced growth cone turning in cultured sensory neurons (for example (Rohm et al., 2000; Takahashi et al., 1999). However, subsequent knockout studies in mice did not confirm a direct role for PLXNA1 in sensory nerve axon guidance (Takegahara et al., 2006). Rather, PLXNA4 was found to be the main physiological co-receptor for NRP1 in several different SEMA3A-mediated axon patterning events, such as sensory nerve fasciculation and sympathetic axon guidance (Cheng et al., 2001; Suto et al., 2005; Yaron et al., 2005). We found that all four A-type plexins were expressed in primary embryonic motor neurons, and that facial motor neurons in situ expressed PLXNA2, PLXNA3 and PLXNA4 (Fig. 1). However, despite its expression in the motor column at r5-level, PLXNA2 was not essential for facial branchiomotor or visceromotor guidance. This observation may indicate that PLXNA2 expression in this domain has no functional significance, or that it plays a role in another type of r5-derived motor neuron, which forms the abducens nerve. On the other hand, PLXNA3 and PLXNA4 were essential for facial nerve development, as both contributed to the patterning of facial branchiomotor axons (Fig. 2); moreover, PLXNA4, but not PLXNA3, controlled facial visceromotor axon guidance (Fig. 4). Accordingly, compound mutants lacking both PLXNA3 and PLXNA4 showed more severe defects in facial branchiomotor neuron patterning, whilst facial visceromotor axon guidance was not affected any worse in these mutants relative to single *Plxna4*-null mutants (compare with 2H, I and 4 H, I with Figs. 6B, D).

It has previously been proposed that PLXNA4 preferentially interacts with NRP1 to form the main SEMA3A receptor, whilst PLXNA3 associates with NRP2 to form the main SEMA3F receptor (Yaron et al., 2005). We have made several observations that support this concept. Firstly, cranial nerve defects in mice lacking SEMA3A or NRP1 are more similar to those of mice lacking PLXNA4, whereas defects in mice lacking SEMA3F or NRP2 are more similar to those of mice lacking PLXNA3 (Fig. 2). Secondly, facial visceromotor neurons respond to SEMA3A and require NRP1 and PLXNA4, but not NRP2 or PLXNA3 for their guidance (Fig. 5). Finally, mutants lacking both PLXNA3 and PLXNA4 show a worse phenotype than single mutants with respect to facial branchiomotor axon guidance, which depends on both SEMA3A and SEMA3F, whereas they do not show a worse phenotype with respect to facial visceromotor neuron patterning, which relies on SEMA3A, but not SEMA3F (Figs. 2, 4, 6). We therefore conclude that SEMA3A/NRP1/PLXNA4 and SEMA3F/NRP2/PLXNA3 pathways co-operate in a non-redundant fashion during facial nerve development (see model in Fig. 6E).

Whilst the *Plxna4*-null facial nerve phenotype was phenocopied in *Sema3a*- or *Nrp1*-null mutants (Figs. 2, 4), SEMA3A/NRP1 may signal through PLXNA3 in other axon types in the mouse (Cheng et al., 2001). Moreover, in zebrafish, SEMA3A1 signals through PLXNA3 to control fasciculation and target selection of VIIth nerve motor axons (Tanaka et al., 2007). Given the essential role of PLXNA3 in mediating semaphorin signals in zebrafish and mouse, it is surprising that the chick genome lacks a PLXNA3 homolog (Mauti et al., 2006). It therefore appears that PLXNA3 and PLXNA4 have undergone species-dependent specialisation to mediate selective axon guidance events, which is exemplified by the requirement for both plexins during distinct aspects of facial nerve development in the mouse (see model in Fig. 6E).

Acknowledgments

We thank Drs Hajime Fujisawa, Masahiko Taniguchi, David D. Ginty and Alex L. Kolodkin for providing mouse strains, Joaquim Vieira for help with genotyping and the staff of the Biological Resources Unit at the UCL Institute of Ophthalmology for help with mouse husbandry. This research was funded by a Career Development Award from the Medical Research Council to C.R. (G120/727) and an a NIH grant (HD045757) to H.W.C.

References

Auclair, F., Valdes, N., Marchand, R., 1996. Rhombomere-specific origin of branchial and visceral motoneurons of the facial nerve in the rat embryo. J. Comp. Neurol. 369, 451–461.

Bagri, A., Cheng, H.J., Yaron, A., Pleasure, S.J., Tessier-Lavigne, M., 2003. Stereotyped pruning of long hippocampal axon branches triggered by retraction inducers of the semaphorin family. Cell 113, 285–299.

Chedotal, A., Del Rio, J.A., Ruiz, M., He, Z., Borrell, V., de Castro, F., Ezan, F., Goodman, C.S., Tessier-Lavigne, M., Sotelo, C., Soriano, E., 1998. Semaphorins III and IV repel hippocampal axons via two distinct receptors. Development 125, 4313–4323.

Chen, H., Chedotal, A., He, Z., Goodman, C.S., Tessier-Lavigne, M., 1997. Neuropilin-2, a novel member of the neuropilin family, is a high affinity receptor for the semaphorins Sema E and Sema IV but not Sema III. Neuron 19, 547–559.

Chen, H., Bagri, A., Zupicich, J.A., Zou, Y., Stoeckli, E., Pleasure, S.J., Lowenstein, D.H., Skarnes, W.C., Chedotal, A., Tessier-Lavigne, M., 2000. Neuropilin-2 regulates the development of selective cranial and sensory nerves and hippocampal mossy fiber projections. Neuron 25, 43–56.

Cheng, H.J., Bagri, A., Yaron, A., Stein, E., Pleasure, S.J., Tessier-Lavigne, M., 2001. Plexin-A3 mediates semaphorin signaling and regulates the development of hippocampal axonal projections. Neuron 32, 249–263.

Cordes, S.P., 2001. Molecular genetics of cranial nerve development in mouse. Nat. Rev. Neurosci. 2, 611–623.

Enomoto, H., Crawford, P.A., Gorodinsky, A., Heuckeroth, R.O., Johnson Jr., E.M., Milbrandt, J., 2001. RET signaling is essential for migration, axonal growth and axon guidance of developing sympathetic neurons. Development 128, 3963–3974.

Feiner, L., Koppel, A.M., Kobayashi, H., Raper, J.A., 1997. Secreted chick semaphorins bind recombinant neuropilin with similar affinities but bind different subsets of neurons in situ. Neuron 19, 539–545.

Giger, R.J., Cloutier, J.F., Sahay, A., Prinjha, R.K., Levengood, D.V., Moore, S.E., Pickering, S., Simmons, D., Rastan, S., Walsh, F.S., Kolodkin, A.L., Ginty, D.D., Geppert, M., 2000. Neuropilin-2 is required in vivo for selective axon guidance responses to secreted semaphorins. Neuron 25, 29–41.

Gu, C., Rodriguez, E.R., Reimert, D.V., Shu, T., Fritzsch, B., Richards, L.J., Kolodkin, A.L., Ginty, D.D., 2003. Neuropilin-1 conveys semaphorin and VEGF signaling during neural and cardiovascular development. Dev. Cell 5, 45–57.

Guidry, G., Landis, S.C., 1995. Sympathetic axons pathfind successfully in the absence of target. J. Neurosci. 15, 7565–7574.

Henderson, C.E., Bloch-Gallego, E., Camu, W., 1995. Purified embryonic motoneurons. In: Cohen, J., Wilkin, G. (Eds.), Nerve Cell Culture: A Practical Approach. IRL Press, Oxford. ISBN: 0199634858.

Jacob, J., Guthrie, S., 2000. Facial visceral motor neurons display specific rhombomere origin and axon pathfinding behavior in the chick. J. Neurosci. 20, 7664–7671.

Jacob, J., Tiveron, M.C., Brunet, J.F., Guthrie, S., 2000. Role of the target in the pathfinding of facial visceral motor axons. Mol. Cell. Neurosci. 16, 14–26.

Kitsukawa, T., Shimizu, M., Sanbo, M., Hirata, T., Taniguchi, M., Bekku, Y., Yagi, T., Fujisawa, H., 1997. Neuropilin-semaphorin III/D-mediated chemorepulsive signals play a crucial role in peripheral nerve projection in mice. Neuron 19, 995–1005.

Lumsden, A., Keynes, R., 1989. Segmental patterns of neuronal development in the chick hindbrain. Nature 337, 424–428.

Luo, Y., Raible, D., Raper, J.A., 1993. Collapsin: a protein in brain that induces the collapse and paralysis of neuronal growth cones. Cell 75, 217–227.

Mauti, O., Sadhu, R., Gemayel, J., Gesemann, M., Stoeckli, E.T., 2006. Expression patterns of plexins and neuropilins are consistent with cooperative and separate functions during neural development. BMC. Dev. Biol. 6, 32.

Mauti, O., Domanitskaya, E., Andermatt, I., Sadhu, R., Stoeckli, E.T., 2007. Semaphorin6A acts as a gate keeper between the central and the peripheral nervous system. Neural Develop. 2, 28.

Messersmith, E.K., Leonardo, E.D., Shatz, C.J., Tessier-Lavigne, M., Goodman, C.S., Kolodkin, A.L., 1995. Semaphorin III can function as a selective chemorepellent to pattern sensory projections in the spinal cord. Neuron 14, 949–959.

Moret, F., Renaudot, C., Bozon, M., Castellani, V., 2007. Semaphorin and neuropilin co-expression in motoneurons sets axon sensitivity to environmental semaphorin sources during motor axon pathfinding. Development 134, 4491–4501.

Morin, X., Cremer, H., Hirsch, M.R., Kapur, R.P., Goridis, C., Brunet, J.F., 1997. Defects in sensory and autonomic ganglia and absence of locus coeruleus in mice deficient for the homeobox gene Phox2a. Neuron 18, 411–423.

Palaisa, K.A., Granato, M., 2007. Analysis of zebrafish sidetracked mutants reveals a novel role for Plexin A3 in intraspinal motor axon guidance. Development 134, 3251–3257.

Renaud, J., Kerjan, G., Sumita, I., Zagar, Y., Georget, V., Kim, D., Fouquet, C., Suda, K., Sanbo, M., Suto, F., Ackerman, S.L., Mitchell, K.J., Fujisawa, H., Chedotal, A., 2008.

Plexin-A2 and its ligand, Sema6A, control nucleus-centrosome coupling in migrating granule cells. Nat. Neurosci. 11, 440–449.
Riddle, R.D., Johnson, R.L., Laufer, E., Tabin, C., 1993. Sonic hedgehog mediates the polarizing activity of the ZPA. Cell 75, 1401–1416.
Rohm, B., Ottemeyer, A., Lohrum, M., Puschel, A.W., 2000. Plexin/neuropilin complexes mediate repulsion by the axonal guidance signal semaphorin 3A. Mech. Dev. 93, 95–104.
Sahay, A., Molliver, M.E., Ginty, D.D., Kolodkin, A.L., 2003. Semaphorin 3F is critical for development of limbic system circuitry and is required in neurons for selective CNS axon guidance events. J. Neurosci. 23, 6671–6680.
Schwarz, Q., Gu, C., Fujisawa, H., Sabelko, K., Gertsenstein, M., Nagy, A., Taniguchi, M., Kolodkin, A.L., Ginty, D.D., Shima, D.T., Ruhrberg, C., 2004. Vascular endothelial growth factor controls neuronal migration and cooperates with Sema3A to pattern distinct compartments of the facial nerve. Genes Dev. 18, 2822–2834.
Schwarz, Q., Vieira, J.M., Howard, B., Eickholt, B.J., Ruhrberg, C., 2008. Neuropilin 1 and 2 control cranial gangliogenesis and axon guidance through neural crest cells. Development 135, 1605–1613.
Studer, M., Lumsden, A., Ariza-McNaughton, L., Bradley, A., Krumlauf, R., 1996. Altered segmental identity and abnormal migration of motor neurons in mice lacking Hoxb-1. Nature 384, 630–634.
Suto, F., Murakami, Y., Nakamura, F., Goshima, Y., Fujisawa, H., 2003. Identification and characterization of a novel mouse plexin, plexin-A4. Mech. Dev. 120, 385–396.
Suto, F., Ito, K., Uemura, M., Shimizu, M., Shinkawa, Y., Sanbo, M., Shinoda, T., Tsuboi, M., Takashima, S., Yagi, T., Fujisawa, H., 2005. Plexin-a4 mediates axon-repulsive activities of both secreted and transmembrane semaphorins and plays roles in nerve fiber guidance. J. Neurosci. 25, 3628–3637.
Suto, F., Tsuboi, M., Kamiya, H., Mizuno, H., Kiyama, Y., Komai, S., Shimizu, M., Sanbo, M., Yagi, T., Hiromi, Y., Chedotal, A., Mitchell, K.J., Manabe, T., Fujisawa, H., 2007. Interactions between plexin-A2, plexin-A4, and semaphorin 6A control lamina-restricted projection of hippocampal mossy fibers. Neuron 53, 535–547.
Takahashi, T., Strittmatter, S.M., 2001. Plexina1 autoinhibition by the plexin sema domain. Neuron 29, 429–439.
Takahashi, T., Fournier, A., Nakamura, F., Wang, L.H., Murakami, Y., Kalb, R.G., Fujisawa, H., Strittmatter, S.M., 1999. Plexin-neuropilin-1 complexes form functional semaphorin-3A receptors. Cell 99, 59–69.
Takegahara, N., Takamatsu, H., Toyofuku, T., Tsujimura, T., Okuno, T., Yukawa, K., Mizui, M., Yamamoto, M., Prasad, D.V., Suzuki, K., Ishii, M., Terai, K., Moriya, M., Nakatsuji, Y., Sakoda, S., Sato, S., Akira, S., Takeda, K., Inui, M., Takai, T., Ikawa, M., Okabe, M., Kumanogoh, A., Kikutani, H., 2006. Plexin-A1 and its interaction with DAP12 in immune responses and bone homeostasis. Nat. Cell. Biol. 8, 615–622.
Tamagnone, L., Artigiani, S., Chen, H., He, Z., Ming, G.I., Song, H., Chedotal, A., Winberg, M.L., Goodman, C.S., Poo, M., Tessier-Lavigne, M., Comoglio, P.M., 1999. Plexins are a large family of receptors for transmembrane, secreted, and GPI-anchored semaphorins in vertebrates. Cell 99, 71–80.
Tanaka, H., Maeda, R., Shoji, W., Wada, H., Masai, I., Shiraki, T., Kobayashi, M., Nakayama, R., Okamoto, H., 2007. Novel mutations affecting axon guidance in zebrafish and a role for plexin signalling in the guidance of trigeminal and facial nerve axons. Development 134, 3259–3269.
Taniguchi, M., Yuasa, S., Fujisawa, H., Naruse, I., Saga, S., Mishina, M., Yagi, T., 1997. Disruption of semaphorin III/D gene causes severe abnormality in peripheral nerve projection. Neuron 19, 519–530.
Tiveron, M.C., Hirsch, M.R., Brunet, J.F., 1996. The expression pattern of the transcription factor Phox2 delineates synaptic pathways of the autonomic nervous system. J. Neurosci. 16, 7649–7660.
Traboulsi, E.I., 2007. Congenital cranial dysinnervation disorders and more. J. Aapos. 11, 215–217.
Waimey, K.E., Huang, P.H., Chen, M., Cheng, H.J., 2008. Plexin-A3 and plexin-A4 restrict the migration of sympathetic neurons but not their neural crest precursors. Dev. Biol. 315, 448–458.
Yaron, A., Huang, P.H., Cheng, H.J., Tessier-Lavigne, M., 2005. Differential requirement for Plexin-A3 and -A4 in mediating responses of sensory and sympathetic neurons to distinct class 3 Semaphorins. Neuron 45, 513–523.
Yip, J.W., 1987. Target cues are not required for the guidance of sympathetic preganglionic axons. Brain Res. 429, 155–159.

Developmental Biology 321 (2008) 251–262

Contents lists available at ScienceDirect

Developmental Biology

journal homepage: www.elsevier.com/developmentalbiology

Repulsive and attractive semaphorins cooperate to direct the navigation of cardiac neural crest cells

Toshihiko Toyofuku [a,c,g,*], Junko Yoshida [b,g], Tamiko Sugimoto [b], Midori Yamamoto [b], Nobuhiko Makino [a,d], Hyota Takamatsu [a,c], Noriko Takegahara [a,c], Fumikazu Suto [e], Masatsugu Hori [d], Hajime Fujisawa [f], Atsushi Kumanogoh [a,c,g,*], Hitoshi Kikutani [b,c,g]

[a] Department of Immunopathology, Research Institute for Microbial Diseases, Osaka University, 3-1 Yamada-oka, Suita, Osaka 565-0871, Japan
[b] Department of Molecular Immunology, Research Institute for Microbial Diseases, Osaka University, 3-1 Yamada-oka, Suita, Osaka 565-0871, Japan
[c] World Premier International Immunology Frontier Research Center, Osaka University, 3-1 Yamada-oka, Suita, Osaka 565-0871, Japan
[d] Department of Cardiovascular Medicine, Osaka University Graduate School of Medicine, 2-2 Yamada-oka, Suita, Osaka 565-0871, Japan
[e] Division of Developmental Genetics, National Institute of Genetics, Mishima 411-8540, Japan
[f] Division of Biological Science, Nagoya University Graduate School of Science, Chikusa-ku, Nagoya 464-8602, Japan
[g] CREST, Japan Science and Technology Corporation, Japan

ARTICLE INFO

Article history:
Received for publication 9 January 2008
Revised 18 June 2008
Accepted 18 June 2008
Available online 30 June 2008

Keywords:
Semaphorin
Cardiac neural crest
Neuropilins
Plexin

ABSTRACT

The cardiac neural crest, a subpopulation of the neural crest, contributes to the cardiac outflow tract formation during development. However, how it follows the defined long-range migratory pathway remains unclear. We show here that the migrating cardiac neural crest cells (NCCs) express Plexin-A2, Plexin-D1 and Neuropilin. The membrane-bound ligands for Plexin-A2, Semaphorin (Sema)6A and Sema6B, are expressed in the dorsal neural tube and the lateral pharyngeal arch mesenchyme (the NCC "routes"). Sema3C, a ligand for Plexin-D1/neuropilin-1, is expressed in the cardiac outflow tract (the NCC "target"). Sema6A and Sema6B repel neural crest cells, while Sema3C attracts neural crest cells. Sema6A and Sema6B repulsion and Sema3C attraction are diminished either when Plexin-A2 and Neuropilin-1, or when Plexin-D1, respectively, are knocked down in NCCs. When RNAi knockdown diminishes each receptor in NCCs, the NCCs fail to migrate into the cardiac outflow tract in the developing chick embryo. Furthermore, Plexin-A2-deficient mice exhibit defects of cardiac outflow tract formation. We therefore conclude that the coordination of repulsive cues provided by Sema6A/Sema6B through Plexin-A2 paired with the attractive cue by Sema3C through Plexin-D1 is required for the precise navigation of migrating cardiac NCCs.

Introduction

The neural crest is a cellular population contained within the leading edge of the neural folds. These neural crest cells (NCCs) migrate to various tissues in a segmented manner in the developing vertebrate embryo when neural tube closes. Depending on their precise destination within the embryo, NCCs generate neurons, glia, pigment cells, chondrocytes and smooth muscle cells (Gammill and Bronner-Fraser, 2003; Le Douarin et al., 2004). After delaminating from the neural tube, NCCs at the level of rhombomeres (r)6 to r8 migrate ventrally and form third, fourth, and sixth pharyngeal arch arteries to the cardiac outflow tract. There, they then fuse to form the septum dividing the single great vessel emerging from the heart (the truncus arteriosus) into the mature aortic and pulmonary arteries, leading to their destination as the cardiac NCCs (Creazzo et al., 1998; Etchevers et al., 2001; Stoller and Epstein, 2005). These columns of cells contribute to the significant cell mass of the endocardial cushions in the outflow tract (Epstein et al., 2000). When cardiac NCCs are ablated in the chick embryo, various malformations including persistent truncus arteriosus and the absence of various combinations of the third, fourth, and sixth pharyngeal arch arteries occur (Kirby et al., 1983; Waldo et al., 1998). Thus, alterations in this complex developmental program lead to a spectrum of pathologies involving the cardiac outflow and the great arteries that are associated with common forms of congenital heart diseases observed in humans (Gruber and Epstein, 2004).

An unresolved issue in neural crest development is how the NCCs establish their precise pathfinding to distinct target organs. Several lines of evidence have shown a role for axon guidance molecules, including ephrin and semaphorin, in NCC migration along the trunk region (Krull et al., 1997; Wang and Anderson, 1997; Eickholt et al., 1999; Santiago and Erickson, 2002). The trunk NCC ventral route is defined by the inhibitory ephrin expression from the dorsal region (Santiago and Erickson, 2002), while NCC segmental organization is defined by the expression of inhibitory class 3 semaphorins, Sema3A

* Corresponding authors. Department of Immunopathology, Research Institute for Microbial Diseases, Osaka University, 3-1 Yamada-oka, Suita, Osaka 565-0871, Japan.
E-mail addresses: toyofuku@ragtime.biken.osaka-u.ac.jp (T. Toyofuku), kumanogo@ragtime.biken.osaka-u.ac.jp (A. Kumanogoh).

0012-1606/$ – see front matter © 2008 Elsevier Inc. All rights reserved.
doi:10.1016/j.ydbio.2008.06.028

and Sema3F, located in the odd-numbered rhombomeres (r1, r3, and r5) (Osborne et al., 2005; Gammill et al., 2006). In contrast, relatively little is known about the molecular mechanisms that are responsible for the cardiac NCC migration to the cardiac outflow tract. A wide variety of extrinsic and intrinsic programs have been implicated in the cardiac NCC fate decision (Stoller and Epstein, 2005). Mice lacking these factors typically exhibit the interruption of the aortic arch and persistent truncus arteriosus. A similar phenotype has been observed in mice lacking Sema3C (Feiner et al., 2001), Neuropilin-1 (a receptor for class 3 semaphorins) (Kawasaki et al., 1999), or Plexin-D1 (a receptor or co-receptor for class 3 semaphorins) (Gitler et al., 2004; Gu et al., 2005). Zebrafish lacking Sema3D in NCC or Plexin-D1 in vascular endothelial cells also exhibit the impaired cardiac development (Sato et al., 2006; Torres-Vazquez et al., 2004). These results suggested that the class 3 semaphorin-mediated signal is involved in cardiac outflow tract formation. However, it remains unclear whether these defects are caused by abnormalities in migration of NCCs. Furthermore, neither ligands for plexin-A2 nor receptors for Sema3C in the cardiac outflow tract formation have not been determined.

In order to determine the molecular mechanisms underlying how semaphorins regulate the pathfinding of migrating cardiac NCCs, we investigated the semaphorin receptors and their ligands during NCC development. In NCCs, we identified an initial and a continuous expression of Plexin-A2 and the subsequent expression of Neuropilin-1 and Plexin-D1. Concomitant with the spatiotemporal expression of these receptors, the Plexin-A2 ligands Sema6A and Sema6B were expressed as contact repellents along the migratory routes. Sema3C, the ligand for the Neuropilin-1/Plexin-D1 complex, was expressed as a diffusible attractant at the cardiac outflow tract. Perturbation of ligand or receptor expression blocked the proper NCC migration into the cardiac outflow tract. Thus, these results indicate that the cooperation of an attractant at the front and a repellent in the back of the migrating NCCs generates a polarized guidance output along the long-range migratory pathway.

Materials and methods

Plexin-A2 and Plexin-A4 knockout mice

Generation and genotyping of the Plexin-A4$^{-/-}$ alleles or the Plexin-A2$^{-/-}$ alleles have been previously described (Suto et al., 2005, 2007). Mice were backcrossed for eight generations into the C57B6 background. All animal procedures were carried out in accordance with institutional guidelines.

Construction of cDNAs and transfections

Mouse Neuropilin-1 and Plexin-D1 cDNAs have been described previously (Toyofuku et al., 2004b, 2007). Mouse Sema3C and Plexin-A2 cDNAs lacking stop codons were synthesized by PCR, and then were ligated into the pcDNA3.1/V5-HisA (Invitrogen) and pFLAG-CMV-3 (Sigma) expression vectors, resulting in the production of V5-tagged Sema3C and Flag-tagged Plexin-A2, respectively. Sema6A and 6B cDNAs lacking N-terminal signal sequences were synthesized by PCR, and then ligated into pcDNA4/His/Max-A, resulting in the production of Xpress-tagged Sema6A and Sema6B. Resulting plasmids were transfected into HEK293 cells by Fugene-6-mediated transfection (Roche Molecular Biochemicals). Stable cell lines that overexpress the plasmid encoded proteins were established by selection with 800 μg/ml G418 (Sigma).

Production of soluble recombinant proteins

To produce soluble Fc-fused proteins, the extracellular domains of Sema6A and Sema6B, and the full-length Sema3C, cDNAs were ligated into the pEFBos human IgG1 Fc cassette (Suda and Nagata, 1994). These constructs were then transfected into P3U1 plasmacytoma cells by electroporation. Fc-fused proteins were purified from culture supernatants using protein-G sepharose (Pharmacia).

Generation of RNA interference-based knockdown vector and adenovirus

To suppress selected target proteins for loss-of-function analyses, RNA interference (RNAi) was used. For RNAi plasmid construction to direct the synthesis of short hairpin (sh)RNA, DNA templates for the synthesis of shRNAs in which the sense and anti-sense sequences targeting cPlexin-A2, cNeuropilin-1, or cPlexin-D1 were linked with a 9-nucleotide loop (Table S1) were synthesized, and then paired oligonucleotides were annealed and ligated into the pRNAT-H1.1/shuttle (GenScript Co. NJ). For the construction of adenoviral vectors that direct the synthesis of shRNA (RNAi adenovirus), the expression cassette of the pRNAT-H1.1/shuttle encoding respective shRNA (RNAi plasmid) was excised and ligated into BD Adeno-X viral DNA (BD Biosciences Clontech). After transfection of adenoviral vector into HEK293 cells, adenovirus-containing medium was collected and concentrated.

Semaphorin-alkaline phosphatase binding assay

Semaphorin-alkaline phosphatase binding assays were performed as described previously (Tamagnone et al., 1999). The extracellular domains of Sema3C, Sema6A, or Sema6B were expressed as fusion proteins with placental secreted alkaline phosphatase at the N-terminus (AP-Sema3C, AP-Sema6A, AP-Sema6B). To assess binding, HEK293 cells were transiently transfected with expression vectors encoding Plexins and NP1. After incubation with AP-Sema proteins, cells were fixed and incubated at 65 °C for 100 min to inactivate endogenous AP activity. Cells expressing Plexin, which bound to AP-Sema, were detected histologically.

Surface biotinylation-chase experiment

HEK293 cells expressing Sema6A or Sema6B were biotinylated using a Cellular Labeling and Immunoprecipitation kit (Boehringer Mannheim). After biotinylation, the culture supernatants and the cells were harvested at the indicated times, washed and solubilized in 1% NP-40, after which they were centrifuged at 100,000 ×*g* for 1 h to remove membrane debris. The contents of the remaining supernatants and cell lysates were immunoprecipitated with streptavidin and subjected to SDS-PAGE. The immunoblots were probed with anti-Xpress-HRP conjugates (Invitrogen) and developed using ECL reagent (Amersham Pharmacia Biotech, Uppsala, Sweden).

Neural crest explant culture and stripe assay

Neural crest explant cultures were performed as described previously (Eickholt et al., 1999). Briefly, neural tube extending from the mid-optic placode to the 3rd somite, from which the robust migration of cardiac NCCs occur, were dissected from chick embryos at stage 9 and incubated for 5 min in Dispase (1 mg/ml in L-15) to remove the mesenchyme and the notochord. For the stripe assay (Eickholt et al., 1999; Vielmetter et al., 1990), neural tube explants were placed on coverslips which had been coated with alternating substratum stripes. Briefly, poly-L-lysine-coated coverslips were placed on silicone matrices. A mix of the purified Sema3C-Fc, Sema6A-Fc, Sema6B-Fc, or control IgG (80 μg/ml) plus fibronectin (1 μg/ml) in PBS was injected into canal and incubated for 3 h at 37 °C. After removing unbound proteins by PBS injection, BSA-FITC was injected into the canal and incubated for 1 h at 37 °C. Coverslips were then removed from matrix, washed with PBS, and then incubated with fibronectin (10 μg/ml) for 3 h at 37 °C. Neural tube explants were cultured on striped substrata for 20 h and examined with anti-HNK-1 antibody (Zymed, 1:100) followed by Rhodamine-conjugated anti-mouse IgG. For adenovirus-mediated